UNIVERSITY OF CALIFORNIA,
IRVINE

Effects of Spark Plasma Sintering on Binary Diffusion of Beta Phase Ti-Nb

THESIS

Submitted in partial satisfaction of the requirements for the degree of

MASTER OF SCIENCE

in

Material Science and Engineering

by

Stoney Alexander Middleton

Thesis Committee:
Distinguished Professor Enrique J. Lavernia, Chair
Professor James C. Earthman
Professor Daniel R. Mumm

2018

DEDICATION

To

My parents, Mark and Linda,

And my wife, Kathleen

TABLE OF CONTENTS

LIST OF FIGURES

LIST OF TABLES

ACKNOWLEDGMENTS

I would like to thank the following individuals who have given their time and expertise to assist my education.

Firstly, I would like to express my gratitude to my advisor Enrique Lavernia for his kind advice, encouragement, and thoughtful guidance.

My committee members James Earthman and Daniel Mumm for their roles as educators during my graduate and undergraduate coursework.

Darryl Mack for timely help with experimental issues. His expertise in laboratory equipment seems to have no bounds.

Aparna Tripathi and Kaustubh Kulkarni for their helpful counsel.

James Haley for consistently providing thoughtful assistance with both experimental and theoretical difficulties.

Alex Dupuy for his valuable mentorship, guidance, and knowledge.

Ben Macdonald for being a source of comradery and motivation.

All my colleagues in the Lavernia and Schoenung laboratory.

My family and friends for their positive encouragement.

The National Science Foundation for their gracious financial support.

ABSTRACT

Effects of Spark Plasma Sintering on Binary Diffusion of Beta Phase Ti-Nb

By

Stoney Alexander Middleton

Master of Science in Material Science and Engineering

University of California, Irvine, 2018

Professor Enrique J. Lavernia, Chair

Interest in titanium for mass-scale applications has driven an exploration for rapid, cost-effective consolidation of titanium powders. The effects of electric current and pressure on binary diffusion in beta phase titanium niobium are studied to enhance understanding of Spark Plasma Sintering (SPS), an advanced powder consolidation technology. Binary diffusion couples were annealed in the SPS system, as well as a custom-fabricated load-free furnace, for one hour to elucidate the influences of pressure and current at 1000, 1100, and 1150°C. The results show Ti-Nb interdiffusion coefficient dependence on composition, temperature, current, and pressure. Compared to published results, the activation energy for low concentration Nb, 10-22 at%, has shown to be reduced in the SPS by an average 38kJmol^{-1} at 15MPa and 70kJmol^{-1} at 80MPa. The effect on activation energy of direct current without pressure, at a similar current density as the SPS, shows an average decrease of 105kJmol^{-1}. The possible mechanisms for these changes are discussed, and concepts for subsequent studies are provided.

CHAPTER ONE

Introduction and Background

The main goal of this work is to investigate the changes in diffusion properties of Ti and Nb during diffusion annealing under electric current and pressure. This data will aid in understanding the key SPS parameters, temperature and pressure, and diffusion mechanisms for Ti-Nb in the SPS. The Ti-Nb-Al material properties have been found to be sufficiently useful for automotive purposes which have initiated research in advanced processing of these alloys. SPS is a powder consolidation technology that uses electric current and pressure to rapidly densify all types of material powders and has shown potential for titanium powder metallurgy [1]. This work will examine the effects of the SPS system to better understand the diffusional mechanisms taking place by investigating electric current, current direction, and combined pressure and current on the binary Ti-Nb system. The effects of SPS on Ti-Nb will provide a useful understanding of single-phase solid solution interdiffusion in the SPS. To provide a perspective for the resulting analysis a review is given on the following subjects: Ti-Nb-Al background, Ti-Nb-Al and Ti-Nb properties, interdiffusion and electromigration theory, and software used to calculate interdiffusion coefficients.

1.1 Motivation

Titanium and its alloys offer mechanical and physical properties which make it an excellent choice for many engineering applications, yet its cost keeps mass automotive manufacturers at a distance. The value of titanium alloys has been well known since the Cold War where it was stockpiled and safeguarded due to its beneficial properties for

defense applications [2]. Nearly 30 years later, titanium alloys can be found in numerous commercial applications such as space, aircraft, biomedical, and specialty equipment [1][3]. However, automotive titanium components are limited from the high cost associated with two different processing categories: raw material synthesis, and post-processing forging and milling [4]. Titanium's large expense is a direct result of its reactivity in ambient environments which makes large-scale vacuum systems and special handling a requirement during high temperature processing stages [3]. For example, titanium compared to aluminum is five times more expensive to refine and ten times more expensive to form per cubic inch [2]. However, a recent study, published in 2010, provides a new electrolytic titanium powder production process that would reduce commercially pure titanium powder costs by 50%. Funded by DARPA, the electrolytic process converts titanium dioxide into commercially pure titanium[4]. The scalability of this process is still underway, but if successful would lead to an increase in inexpensive commercially pure titanium powder.

With economical titanium powder on the horizon, there is increased incentive to investigate advanced powder metallurgy routes such as current-assisted sintering which includes SPS. In general, powder metallurgy also removes two costly steps in manufacturing, gas atomization of Ti sponge and forging [2][1]. SPS is a rapid powder consolidation technique that creates fully dense near-net shape forms. Additionally, SPS has been shown to have certain advantages compared to other powder metallurgy methods such as lower sintering temperatures, shorter hold times, and improved mechanical performance [5]. Moreover, SPS experiments conducted on blended elemental titanium aluminum powder has been shown to decrease the activation energies for intermetallic

formation [6]. The advantages of SPS and the promise of inexpensive titanium powder has likely motivated a patent by General Motors Company for processing titanium aluminide powders with field assisted sintering technologies [7]. However, there is still a lack of knowledge for the multicomponent thermodynamic and kinetic properties under SPS conditions. In order for current-assisted sintering to become a viable method for the automotive industry a detailed understanding of material characteristics during SPS processing and the ability to model such methods is key.

The present work focuses on the combined effects that electric current and pressure have on diffusion properties of beta phase Ti-Nb in the SPS system. There have been several reviews on the fundamentals of field assisted sintering technologies [5][8][9][10]. Although many of these reviews are in the scope of powder densification and sintering properties. The factors that govern mass transfer during SPS are assessed later including temperature, current, and pressure. The Ti-Nb system is well studied with authors providing impurity, self, and interdiffusion coefficients [11]. Though there is still a gap in knowledge, no studies have been found that systematically study the diffusion properties of Beta phase Ti-Nb during SPS. Additionally, an experimental apparatus which also applies current to a diffusion couple is used to elucidate current effects without any applied load. Ultimately, this study will provide data that will be comparable to the Ti-Nb work already available to investigate mass transfer in SPS. This study also aims to provide an experimental methodology that could be used on the Ti-Nb-Al system.

1.2 Ti-Nb-Al Background

A brief highlight of titanium's general features and relevant industrial motivation to study the Ti-Nb-Al and Ti-Nb are provided. Pure titanium has a melting point of 1668°C, a density of 4.506g/cm^3 and is allotropic at 882°C forming a Hexagonal Close Packed (HCP) structure at low temperatures and a Body Centered Cubic (BCC) structure at higher temperatures [12]. Alloying elements for titanium alloys are referred to as alpha stabilizing or beta stabilizing depending on the structure which is favorably formed with their addition. Table 1.1 shows various alloy elements and the phases which they stabilize. The table is organized according to Hume-Rothery rules for substitutional solid solubility which occurs if the atomic radius, crystal structure, and chemical nature are very similar [13]. Seen in Table 1.1, Al is an alpha (HCP) stabilizing constituent while Nb is a beta (BCC) stabilizer. The Ti-Al system forms several intermetallic phases at various compositions and temperatures including Ti_3Al (α_2) , TiAl (γ), and $TiAl_3$ (α) [3]. On the other hand, the Ti-Nb system forms a BCC single phase at high temperature throughout the entire composition range, seen in Figure 1.1. Additionally, the microstructure of Ti-Al intermetallics has been categorized by industry in the following groups; near gamma, duplex, nearly lamellar, and fully lamellar. The fully lamellar and duplex structures have been found useful for several commercial applications due to fatigue resistance and strength, respectively [3]. However, the properties of Ti-Al alone are not acceptable for demanding application in engine environments that are both high temperature and oxygen-rich.

Table 1.1: Common titanium alloying elements and titanium phase stabilized [13]

	Element	Native Crystal form	Atomic Radius (pm)	Common Valence	Electro-negativity	Ti Phase Stabilized
Substitutional Alloy Elements	Titanium	BCC, HCP	140	3,4	1.5	N/A
	Aluminum	FCC	125	3	1.6	Alpha
	Niobium	BCC	145	5	1.6	Beta
	Molybdenum	HCP	145	3,5,6	2.2	Beta
	Iron	FCC, BCC	140	2,3	1.8	Beta
	Silicon	DC	110	4	1.9	Beta
	Vanadium	BCC	135	4,5	1.6	Beta
	Zirconium	BCC, HCP	155	4	1.3	Neutral
	Chromium	BCC	140	3,5,6	1.7	Beta
	Manganese	BCC	140	2,4,7	1.6	Beta
Interstitial Alloy Elements	Oxygen	N/A	60	N/A	N/A	Alpha
	Nitrogen	N/A	65	N/A	N/A	Alpha
	Carbon	N/A	70	N/A	N/A	Alpha

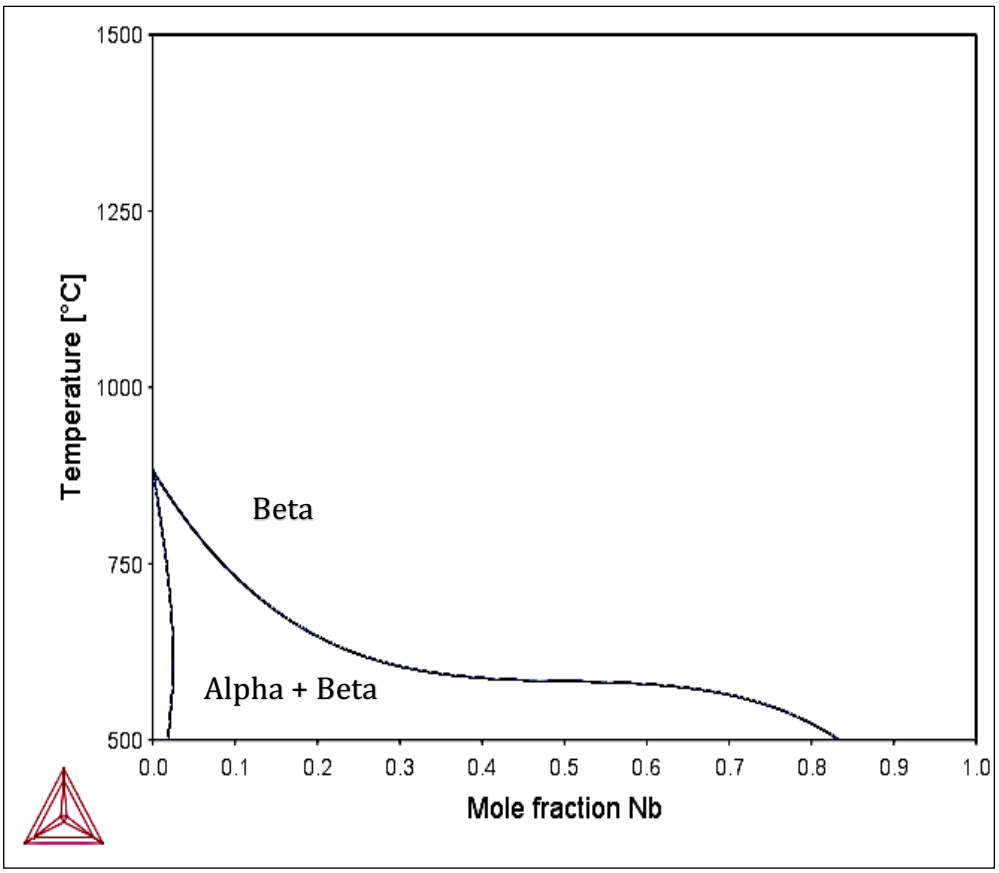

Figure 1.1: The binary Ti-Nb phase diagram calculated with Thermo-Calc

Niobium containing Ti-Al alloys, developed in the 1990's, showed improved strength compared to Inconel 713 and a significant increase in fracture strength, creep resistance, and oxidation resistance [1]. Progress in the development of Ti-Nb-Al alloys has since provided state of the art alloys which can be seen in Table 1.2 [3]. It is worth noting that most of the alloys in Table 1.2 contain 2-10 atomic percent Nb. These alloys make use of Nb effects on creep resistance and fatigue strength attributed to Nb slow diffusion in Ti-Al which lends to the high temperature stabilization of the lamella microstructure [1][3]. Nb is a high temperature performance enhancer because of its solid solution strengthening and short-range order of point defects [3]. However, from a powder metallurgy point of view, these properties make it more difficult to sinter and homogenize by increasing the time needed for Nb diffusion.

The diffusion properties of Ti-Nb and the individual constituents have been studied at length by multiple authors who have collected self, impurity, and interdiffusion coefficients. Ti-Nb self and impurity diffusion work, measured with the isotope tracer method, has shown linear Arrhenius plots meaning the dominant mechanism for diffusion is the normal vacancy mechanism [14][15]. Interdiffusion studies have shown that the diffusion coefficient increases monotonically with increasing titanium concentration in the temperature range of 800-1200C. Recent work by Verma et al. investigated the interdiffusion and activation energy of Ti-Nb at 1100, 1125, and 1150°C annealed for 48, 48, and 24 Hr., respectively, and found the same increasing monotonic behavior of the interdiffusion coefficient with increasing titanium concentration. The activation energy found in Verma's work also shows that as titanium concentration increases the activation energy decreases monotonically [16].

In summary, the Ti-Nb-Al system is industrially useful especially for high temperature application under mechanical loading conditions. Their physical characteristics lead to significant weight savings and thermomechanical benefits that can increase the fuel efficiency of engines making it an excellent material for automotive industry [1]. The low, 1-10 at%, Nb concentration is of particular importance as it is key to the high temperature strengthening mechanisms of Ti-Al and does not overly increase the alloy density. Nb is also the slowest diffusing species in Ti-Nb-Al which has been characterized and verified by several authors making it particularly noteworthy to this study.

Table 1.2: Industrial relevant titanium alloys containing Nb benefits[3]

Alloy Name	Composition (at%)	Key Properties
48-2-2	Ti-48Al-2Cr-2Nb	ductility, fracture toughness, oxidation resistance
Gamma-Met	Ti-45Al-(5-10)Nb	creep, fatigue, high temp. strength, oxidation resistance
TNB Alloy	Ti-(45-47)Al-10Nb	creep, high temp. strength, oxidation resistance
XD TiAl	Ti-45Mn-2Nb-0.8B	ductility, high temp. strength, creep, oxidation resistance

1.3 Binary Interdiffusion

Microstructure changes and their relation to physical properties are key to developing processing methods. Diffusion is the foundation of many structural changes including homogenization, phase transformation and many others making its findings of great importance for mass-produced components. In general, metallic diffusion studies can be divided into 3 groups. First, self-diffusion which is typically measured by a radioactive isotope. Second, binary interdiffusion wherein two elements are annealed then

concentration gradients are quantitatively measured. Finally, multicomponent diffusion encompasses systems of three or more elements measured in the same technique as binary diffusion. The complexity of analysis grows rapidly after the binary system. Typical assumptions that can be applied in binary systems of constant molar volumes and negligible cross interdiffusion terms become inappropriate in multicomponent systems [17]. The classic example of cross interdiffusion terms becoming significant is up-hill diffusion where a species *i* migrates down a free energy gradient that results in a concentration increase of *i*.

Binary diffusion between two infinite metals takes place when their surfaces are in intimate contact at high temperature. C. Matano, with the help of the Boltzmann parameter, solved Fick's second law, a partial differential equation, which describes how concentration changes with time. This analysis is known as the Matano-Boltzmann method and its derivation can be found in many texts [17][18]. It is important to note that this analysis makes the assumption of constant partial molar volume throughout the experiment. Thus, the total volume of the diffusion couple does not change after annealing. The interdiffusion coefficient dependent on the atomic fraction Nb is given below in Equation 1.

$$\widetilde{D}(N^*) = -\frac{1}{2t}\left(\frac{dx}{dN_{Nb}}\right)_{N^*_{Nb}} \left[\int_{N^-_{Nb}}^{N^*_{Nb}} x dN_{Nb}\right] \quad (1)$$

Where N_{Nb} is the atomic fraction of Nb, x is the composition profile location variable, and t is the diffusion anneal time. Other methods of calculating the binary interdiffusion coefficient are the Den Broeder, Sauer-Friese, and Wagner methods [17]. These approaches are useful for systems that deviate from the constant molar volume assumption.

1.4 Effect of Electric Current on Diffusion

In metallic systems, electromigration is the bulk motion of atomic nuclei generated from the passage electrons. Momentum transferred from the electrons to metal atom nuclei is due to an acceleration of electrons by an electric field [19]. Generally, it has been found that electric current enhances mass transport through electromigration, point defect generation, and enhanced defect mobility [8]. A diffusional flux from electromigration in a multicomponent system can be written as follows.

$$J_i = D_i \frac{c_i}{RT}\left[RT\frac{\partial lnc_i}{\partial x} + FZ_iE\right] \quad (2)$$

Where J_i is the atomic flux species i, D_i is the diffusivity, c_i is the concentration, R is the gas constant, F is Faraday's constant, E is the electric field, and Z_i is the effective charge. The effective charge and the diffusivity changes depending on the intrinsic properties of the solvent species. The electromigration effect has been attributed to altering nucleation, growth, thermodynamic stability, and defect formation in many systems [20][21][22]. Hence, diffusion under an electric current can have a large variability depending on the material system in question. Some studies of electric current on titanium alloys have found microstructural orientation preference, enhanced diffusion coefficients, and decreased activation barriers [23][24][6]. In general, the speed of diffusion at an interface between two metals is limited based on diffusion properties and or reaction kinetics. It has been shown that if an intermetallic is formed the kinetic barrier can hinder or block electromigration effects leading to little or no asymmetry in the concentration gradient in regards to [22].

1.5 Effect of Pressure on Diffusion

For the case of hydrostatic pressure on self-diffusion the diffusion coefficient is found to decrease with increasing pressure [25]. An argument has been made for this phenomenon based on thermodynamic principals which can be explained from a vacancy volume standpoint. Roughly, a vacancy causes an expansion of the crystal lattice about the size of an atom, although there is some lattice relaxation. At equilibrium vacancy concentration, a hydrostatic pressure does work on the system by changing the vacancy volume [25]. Hence, if the mechanism for diffusion varies from single vacancy to di-vacancy the activation volume changes. From equilibrium thermodynamics, the following expression can be derived.

$$\left[\frac{\partial \ln\left(\frac{D}{a^2 \nu}\right)}{\partial P}\right]_T = -\left(\frac{V_{SD}}{RT}\right) \tag{3}$$

Where D is the self-diffusion coefficient, a is jump distance, ν a jump frequency factor, and V_{SD} is the activation volume [25]. This result, can be modified to show the diffusion coefficient dependence on pressure.

$$D(P) = D_o \exp\left(-\frac{PV_{SD}}{RT}\right) \tag{4}$$

Where D_o is the pre-exponential diffusion coefficient, P is pressure, and V_{SD} is the activation volume. From this result it is clear the pressure dependence of the diffusion coefficient follows the Arrhenius type relationship [26]. Furthermore, this expression holds for interdiffusion coefficients which is shown below in a slightly different form.

$$\frac{\partial \ln\left(\tilde{D}\right)}{\partial P} = -\frac{\Delta \tilde{V}}{RT} \tag{5}$$

The interdiffusion activation volume is $\Delta\tilde{V}$. From this negative exponential relationship with the diffusion coefficient, it is clear that a significantly large pressure is needed to decrease the diffusion coefficient [26].

Another effect of pressure is from non-equilibrium pressure gradients or deviatoric stress. In the presence of an elastic non-uniform stress or potential gradient, the total flux will be a product of the free energy gradient and the potential field [25]. The flux relationship, Equation 6, is found for a constant diffusion coefficient under a potential force F. The total combined flux of the free energy gradient, in this case, a composition gradient, and the applied potential is given in Equation 7.

$$J = -\left(\frac{Dc}{kT}\right)\nabla F \tag{6}$$

$$J_{total} = -D\nabla\left[\nabla c + \frac{c\nabla F}{kT}\right] \tag{7}$$

Where J is the flux, D is a constant diffusion coefficient, k is Boltzmann's constant, and ∇F is the pressure gradient. Thus, the result of a potential gradient is to modify the flux, but not change the diffusion coefficient.

A study was performed on the self-diffusion of beta phase Ti at 1000°C under a hydrostatic pressure ranging from 32 to 524MPa to determine activation volume [27]. The activation energy determines the degree of relaxation around lattice defects and deviation in the activation volume relates directly to atomic diffusion mechanism [25]. Although many experimental errors are discussed by the author, the activation volume reveals that the self-diffusion of titanium likely proceeds by a combined mechanism of vacancy movement and short-dislocation-path diffusion. The activation volume reported for Ti is 3.6 cm^3mol^{-1}. Also, these results show the Arrhenius type behavior shown in Equation 4.

The averaged slope over two sets of data shows the Ti self-diffusion coefficient per pressure increment is $-3.6 \times 10^{-8}\ m^2(MPa*s)^{-1}$ [27]. This value indicates that an extremely large hydrostatic pressure is needed to make an appreciable negative effect on self-diffusion of Ti.

1.6 Effect of Field Assisted Sintering on Diffusion

SPS falls into a broader category of sintering technologies deemed current-assisted sintering. The obvious common thread between these methods is the application of electric current to enhance sintering of a powder sample. Subcategories are identified by their mode of electric current frequency, voltage, and current density. The 4 subcategories include resistive sintering, DC, 10-50V, $<1kAcm^{-2}$; electro-consolidation, AC, 10-50 V, $<1kAcm^{-2}$; SPS (also known as Pulsed Electric Current Sintering (PECS), Electric Discharge Sintering (EDS), and other similar names), 10^2-10^8Hz DC, 1-50V, $<1kAcm^{-2}$; and electric discharge compaction, single pulse DC, 1-100Hz, >50V, $>10kAcm^2$ [28]. In addition to electric current, these systems also apply pressure to the specimen. The combination of uniaxial pressure and electric current is an important factor for densifying powders. It has been shown over a wide range of materials (aluminum, silicon, zirconia), in a system similar to the SPS, that the densification rate is pressure dependent and can affect diffusion [29]. This leads to the conclusion that combined pressure and current effects are influential to diffusion in the SPS.

Studies pertaining to mass transfer effects of SPS can be broken into two categories. The first is intermetallic formation typically seen in systems where reaction sintering is taking place [30][6]. Diffusion in these studies is often altered by the kinetic barrier caused

by intermetallic formation and growth. Hence, in intermetallic systems, clear separation of the influence of nucleation and growth versus the magnitude of the current is difficult to deconvolute [31]. Alternately, single phase solid solution systems where nucleation and growth are absent make the investigation of the intrinsic role of current more feasible.

A study was conducted on the Cu-Ni (single phase solid solution) system using a constant low-pressure apparatus. The temperature and current density ranges were from 650-850C, and 0-1000 Acm^{-2}, respectively. The interdiffusion was seen to have an electron wind effect, but only on Cu(-)-Ni(+) current direction. The activation energy was found to have the following trends; decreasing with increasing current density and decreasing Cu concentration, yet constant at low Cu concentration [31]. These findings are attributed to the effects of increased vacancy concentration and defect mobility.

An important aspect of the SPS system when considering diffusion is pressure. As mentioned earlier there are two stress components of interest, hydrostatic and deviatoric stress. Finite element modeling of stress in the SPS has been conducted on Al_2O_3 and was found to only have significant variations in the stress field at the die interface [32]. This change in stress field is found at ~20% the radial distance of the sample. Mismatches in thermal expansion coefficient of the die and sample can further alter this stress.

The major source of work for understanding electromigration is from the microelectronics community. However, a growing field that also takes advantage of mass transfer from electric fields is Electrically Assisted Forming (EAF). This type of forming is similar, application of current and pressure, to SPS but on bulk samples rather than powders and at lower temperatures. The following conclusions are drawn from several experiments summarized in work by Salandro et al. [33].

- Joule heating is greater at defect cores termed “hot spots” which enables enhanced defect mobility. For example, in a pure magnesium crystal, the hot spots created an energy of 29keV at a dislocation core while electron wind effect produced $1.29x10^{-3}$eV.
- Experiments with current and no pressure showed that cold worked materials with increased dislocation densities had an increase in the driving force for dislocation movement. The temperature difference during joule heating at hot spots is generated from the difference in electricidal resistivity between the defect and lattice.
- The combined energy from current plus plastic deformation shows increased dislocation mobility allowing the dislocation to move past lattice obstacles. The net result of enhanced dislocation movement is observed by a delay in void formation and fracture during tensile tests.

1.7 Summary

The industrial relevance of Ti-Nb-Al is found in its high temperature properties derived from a 1-10at% Nb concentration. The Ti-Nb system has been well studied in standard diffusion studies which found the diffusional mechanism to be a normal vacancy method. SPS of Ti-Nb is a good primary look into the interdiffusion behaviors before Ti-Nb-Al because Nb is the slowest diffusion species and will likely be a rate limiter for intermetallic formation. Additionally, there is a lack of experimental SPS studies considering pressure variations on diffusion properties. Overall, the goal of this study is to

characterize the effects of current, pressure, and their combination on binary interdiffusion of Ti-Nb during SPS.

CHAPTER TWO

Experimental Procedures

2.1 Materials

Experimental specimens were fabricated using a three-layer assembly of Nb foil in the middle of two Ti foil layers. This arrangement was chosen to enable the investigation of the influence of DC current directionality, schematically shown in Figures 2.1 and 2.2. The titanium and niobium foils were purchased from Alfa Aesar (Tewksbury, MA) with respective metals basis purity of 99.2% and 99.8%. The thickness of both foils is 1 mm. Circular samples of the foils were cut using Electric Discharge Machining (EDM). Molybdenum foil 0.05mm thickness with metal basis purity of 99.95% was used as a diffusion barrier on the exterior of the couples to hinder diffusion from the graphite punch and die. Boron Nitride, machinable grade AX05, purchased from Saint-Gobain (Amherst, NY) was machined into disks, 19mm diameter 0.6mm thickness, and was used to block current in the SPS system. The Ti, Nb, and Mo disks were cleaned after EDM using an ultrasonic bath in acetone, then isopropyl alcohol.

2.2 Experimental Apparatus

Two experimental apparatus were used in this study, an SPS device and a custom vacuum furnace. Figure 2.1 and 2.2 show schematics of both devices and a photograph of the typical experimental setup.

The SPS used for this study is a Syntex Inc. Dr. Sinter (Japan) SPS System Model: SPS-825S. It uses a DC pulse generator with designated on time 1-99 digits, off time 1-9 digits. Each digit is 2.77msec. A 12 on, 2 off pulse was chosen for all experiments due to its

common use. The temperature was ramped in a two-step method to avoid overshooting the set value. The averaged heating rate is 100°Cmin^{-1} which nominally changed depending on the set value. An inert gas quench system was added to the system to mitigate alpha phase formation. The sample pressure was PID controlled to have the desired pressure at the same time as the chosen hold temperature was reached. The load force was ramped at a maximum rate of 2.4kNmin^{-1}. For two SPS experiments, the current was blocked by boron nitride inserts that were placed between the graphite punches and molybdenum foil.

The temperature was measured in both experimental apparatus via a K-Type thermocouple (Omega, USA). The thermocouples were sheathed in a special high temperature alloy, Omega Super OMEGACLAD XL, and electrically insulated from the sheath by the manufacturer. Prior to installing the thermocouple, its accuracy was checked by melting a lead-based solder and checking the well-known solidification temperature to the thermocouple reading. The thermocouples were found to be within the manufacturer's specification.

The other instrument used in this study is a custom apparatus built for studying electromigration which will be referred to as the Electromigration Furnace (EMF). This system is a water-cooled vacuum chamber equipped with radial heating elements, K-type thermocouple, inert gas quench, Omega PID temperature controller, Xantrex DC power supply, National Instruments data acquisition, and Welch 1402 vacuum pump. A Labview program was used to acquire vacuum pressure, temperature, and sample current during the experiment. This system differs from the SPS in three key ways. First, heat is generated from two sources; heating elements and Joule heating. Second, the DC power supply does not pulse the specimen current like the SPS, rather it is constant. Lastly, there is no

constant uniaxial load put on the sample during annealing. These factors make the EMF ideal for investigating electromigration effects at easily controllable current densities which has been done by previous authors [31].

Once samples were loaded into the EMF a vacuum of at least 1Pa was reached, then the system was backfilled with argon, this was repeated at least 3 times to ensure an inert atmosphere. The electrode was raised removing all pressure on the sample until the desired temperature was reached then the electrode was lowered to the sample until sufficient electrical contact was made. This procedure mitigates electrode thermal expansion from pinching the sample which can cause undesired sample damage. A sight hole in the EMF allowed for user control of electrode position during the experiment.

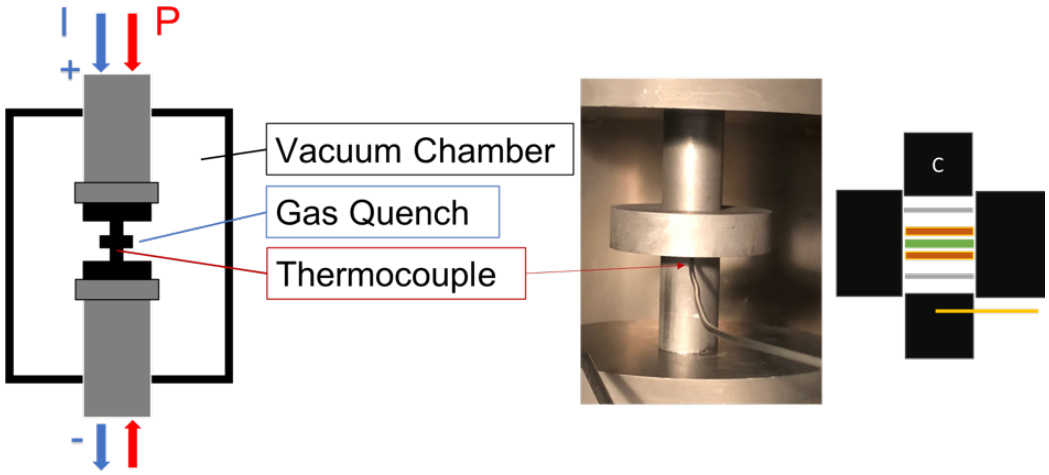

Figure 2.1: Spark Plasma Sintering (SPS) schematic and experimental setup. The gas quench line is off-screen.

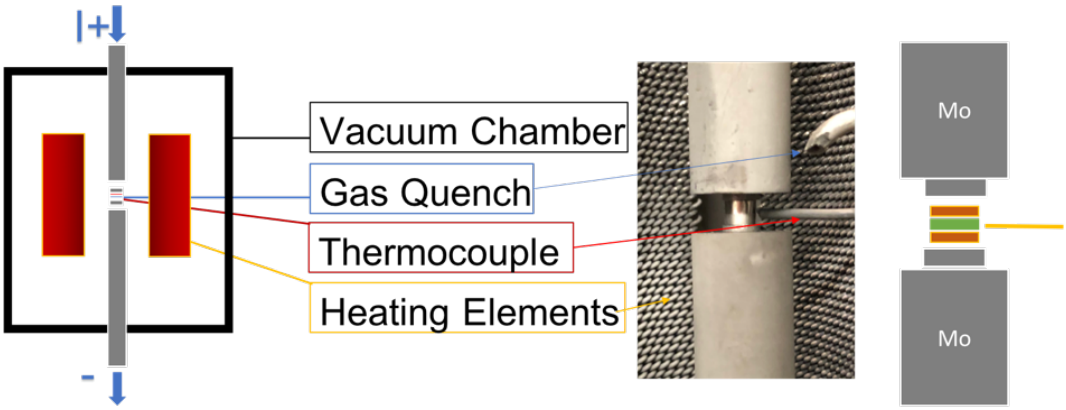

Figure 2.2: Electromigration furnace (EMF) schematic and experimental setup

Scanning Electron Microscope and Electron Probe Micro Analysis (EPMA) were used to obtain micrographs and concentration profiles of the diffusion couples. A Cameca SX-100 EPMA was used to quantitatively measure the Wavelength Dispersive Spectra (WDS). The EPMA process conditions are as follows; 1μm steps size, voltage 15kV, and current 10nA. The Ti, Nb, and Al signals were calibrated using known standards. The WDS detector crystals used were L pentaerythritol (LPET) for Ti Kα1 and Nb Lα1, and L thallium acid phthalate (LTAP) for Al Kα1.

The Ti-Nb diffusion couples were conducted in the SPS and EMF at 3 temperatures 1000, 1100, and 1150°C and two uniaxial pressures 15 and 80MPa. The sample diameter was varied based on the experimental apparatus 19 and 5mm for the SPS and EMF, respectively. The current density was kept constant between the two instruments at 277, 305, and 321Acm^{-2} for the temperatures mentioned. A minimum vacuum level of 1Pa was used to hinder oxidation. A one-hour hold time at temperature was used unless otherwise noted.

At the end of each experiment, the sample was sectioned perpendicular to the diffusion interface using EDM and then mounted in a conductive phenolic resin (Buehler Konductomet) for electron microscopy. The mounted samples were then prepared metallographically by polishing on SiC abrasive paper up to 800 grit then 9μm diamond suspension before a final polishing step using a mixture of colloidal silica plus hydrogen peroxide in a 5:1 volume ratio. The samples were then cleaned using an ultrasonic bath of isopropanol and then air dried to prepare for electron microscopy.

2.3 Flux and Interdiffusion Coefficient Calculation

MultiDiFlux is a computational environment for the analysis of single-phase multicomponent diffusion couples [34]. Experimental composition profiles, typically generated by EPMA, along with user-defined parameters are input into this software to generate several outputs including smoothed concentration profiles, interdiffusion flux, interdiffusion coefficients, and relative error. Smoothing of the experimental concentration data is done by finite element analysis using Hermite interpolation polynomials. The Matano plane, or plane of mass balance, is calculated using Equation 8 from both directions of the concentration profile.

$$\tilde{J}_i = \frac{1}{2t}\int_{C_i^- \text{ or } C_i^+}^{C_i(x)} (x - x_0)\, dC_i \tag{8}$$

Where t is the annealing time, c is the concentration, and x is the location variable. Although, *Multi*DiFlux can calculate compositionally dependent diffusion coefficients the software is limited in the use of averaged diffusion coefficients which were found to deviate from the Matano-Boltzmann method using Equation 1. The interdiffusion coefficients shown throughout this study were calculated using the Matano-Boltzmann method. The

assumption of constant partial molar volume is reasonable due to the closeness of Ti and Nb molar volume 10.621 and 10.841cm^3mol^{-1} respectively. The accuracy of this assumption can be checked by comparing the Matano plane calculation made from integrating the left side or right side of the composition profile. If there is appreciable molar volume change the Matano plane will not be in the same location. In the following experiments there was no appreciable difference found using *Multi*DiFlux Matano plane calculation from the left or right of the concentration profile. Further proving that the assumption of a constant partial molar volume is acceptable.

CHAPTER 3

Results and Analysis

3.1 Binary Diffusion Couples

Table 3.1 shows all the results obtained from the experiments conducted in both systems. Both of the boron nitride current blocking experiments had issues with the thermocouple which resulted in the experiment ending earlier than desired. The annealing time was changed accordingly for the calculation of the interdiffusion coefficient. Averaged temperature and pressure measurements at the set hold temperature with the standard deviations. The Omega K-type thermocouples used have an accuracy of ± 2°C which is greater than any of the measured standard deviations in the work shown in Table 3.1. Thus, the set temperatures are used for all calculations.

Figures 3.1-3.20 provide the following data set for the experiments shown in Table 3.1; SEM micrograph of the interdiffusion interface, the EPMA concentration profile with overlaid *Multi*DiFlux fit, the interdiffusion flux calculated using *Multi*DiFlux, and the interdiffusion coefficient as a function of atomic fraction Nb. The interdiffusion coefficient was calculated in units of m^2s^{-1}. The polarity of the current direction is identified on the diffusion interface micrograph. The Matano plane calculated via *Multi*DiFlux is signified with a dashed line and x_o in both the composition and flux plots.

Alpha stabilization was observed on all samples where Ti was in contact with the graphite die or exposed to an inert atmosphere in the EMF. These microstructures were far (>0.5mm) from the diffusion interface measured with EPMA. The stabilization is the result

of interstitial diffusion of small elements found in Table 1.1; specifically, oxygen, carbon, or nitrogen. This finding is ignored due to its lack of relevance to the present study.

Table 2.1: Experimental parameters for Ti-Nb diffusion couples and notes

Name	Temperature (°C)		Pressure (MPa)		Hold Time (min)	Average Current Density (A/cm^2)	Notes
	Set	Avg.	Set	Avg.			
SPS-1	1000	1000.5 ± 0.3	15	15.3	60	277.7	
SPS-2	1000	1000.3 ± 0.3	80	79.5	60	278.8	
SPS-3	1100	1100.6 ± 0.2	15	15.1	60	306.8	
SPS-4	1100	1100.9 ± 0.3	80	78.4	60	305.6	
SPS-BN-1	1100	1101.3 ± 0.2	15	15.5	52	Boron nitride current blocked	Experiment ended early, thermocouple slipped out of punch.
SPS-BN-2	1100	1101.1 ± 0.2	80	80.4	58	Boron nitride current blocked	Experiment ended early, Thermocouple short circuited on the die.
SPS-5	1150	1150.7 ± 0.2	15	15	60	320.9	
SPS-6	1150	1150.7 ± 0.2	80	78.4	60	322.6	
EMF-1	1000	999.9 ± 0.3	N/A	N/A	60	274.5 ± 0.02	
EMF-2	1100	1099.9 ± 0.1	N/A	N/A	60	305 ± 0.03	
EMF-3	1150	1150 ± 1	N/A	N/A	60	325.6 ± 0.03	

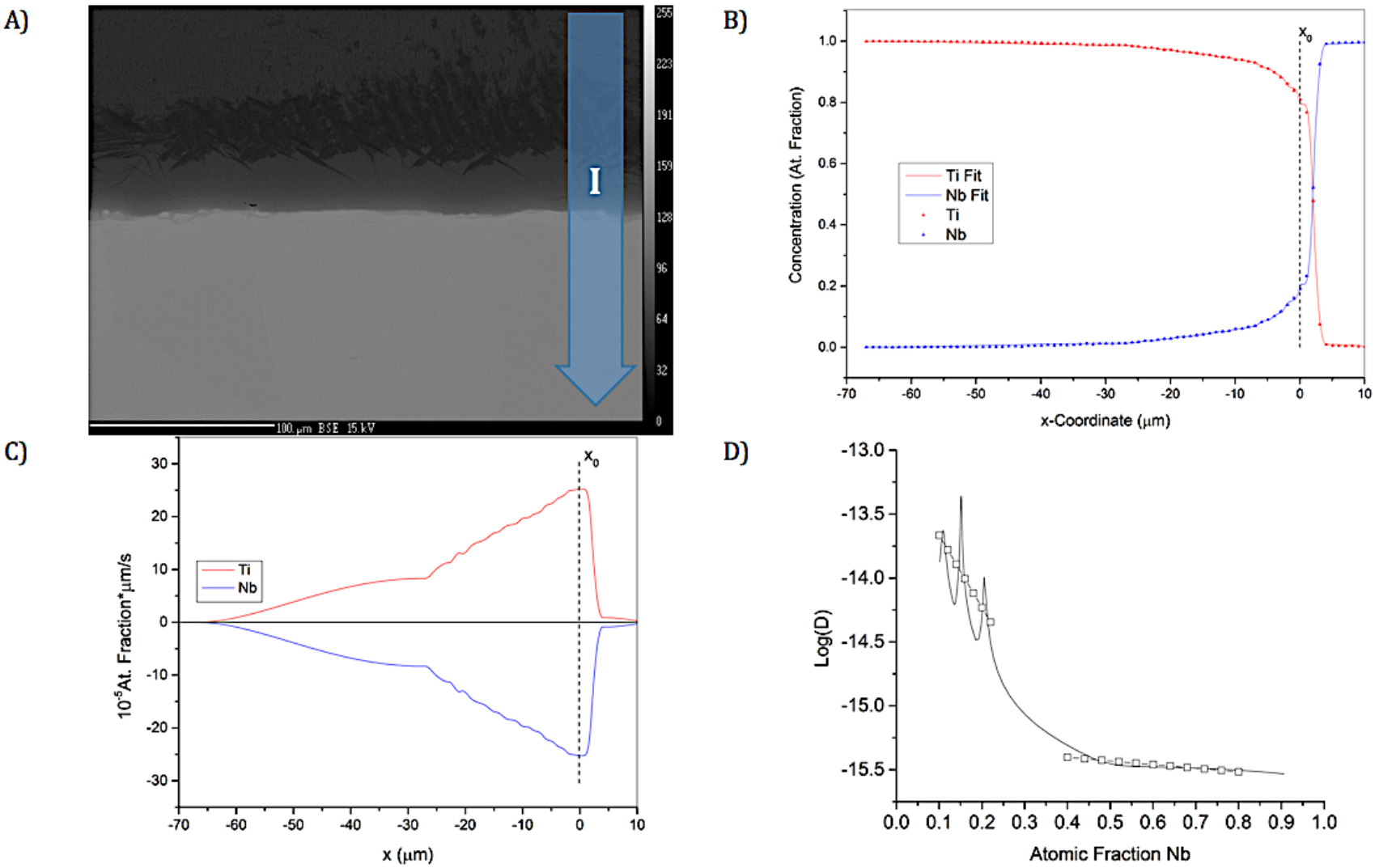

Figure 3.1: SPS-1 1000°C 15MPa Ti(+)-Nb(-) A) SEM BSE micrograph of interdiffusion interface, B) Concentration measurement from EPMA with *Multi*DiFlux fit overlapping, C) Interdiffusion flux calculated from *Multi*DiFlux, D) Interdiffusion coefficient calculated using Matano-Boltzmann method with linear approximations.

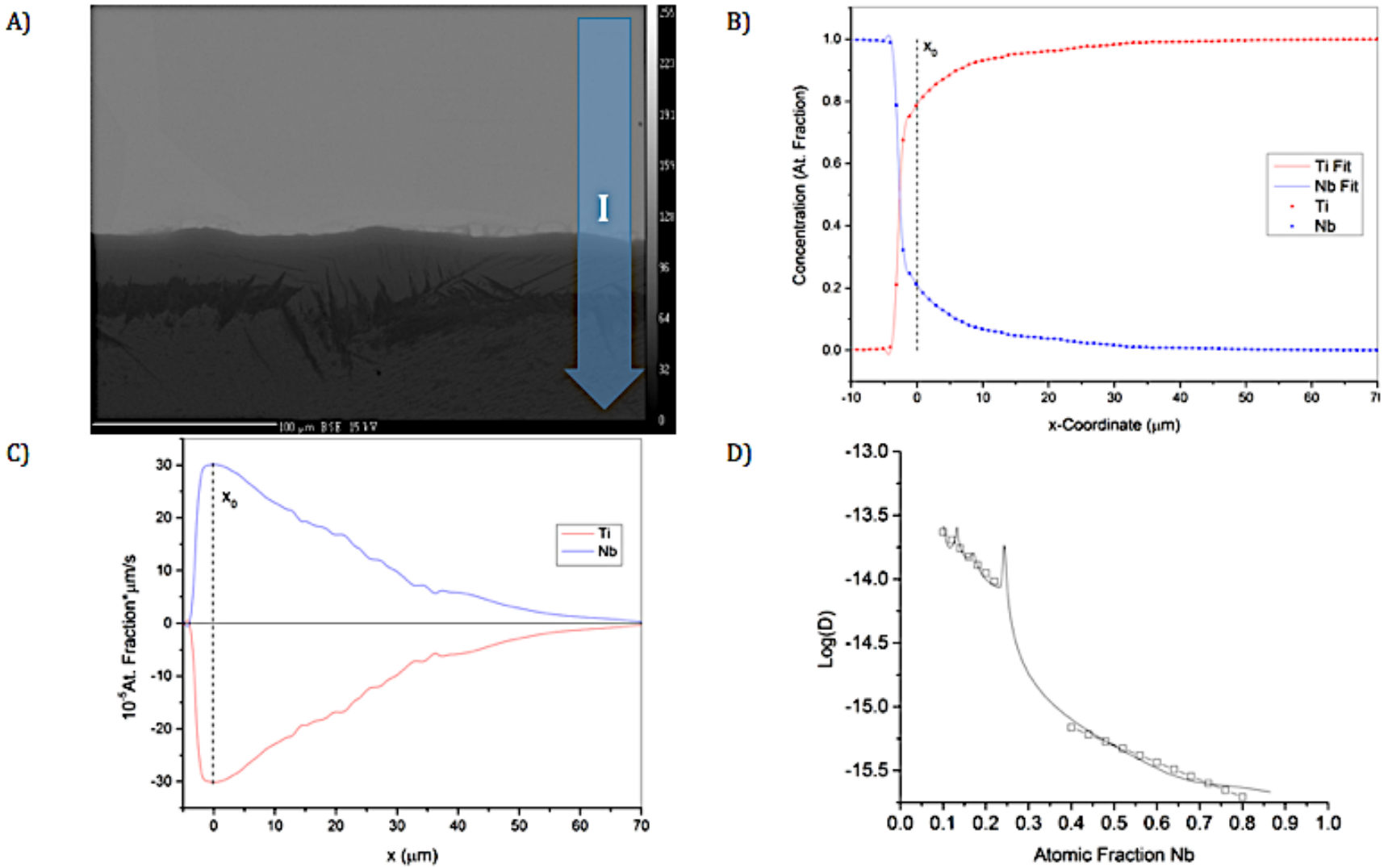

Figure 3.2: SPS-1 1000°C 15MPa Ti(-)-Nb(+) A) SEM BSE micrograph of interdiffusion interface, B) Concentration measurement from EPMA with *Multi*DiFlux fit overlapping, C) Interdiffusion flux calculated from *Multi*DiFlux, D) Interdiffusion coefficient calculated using Matano-Boltzmann method with linear approximations.

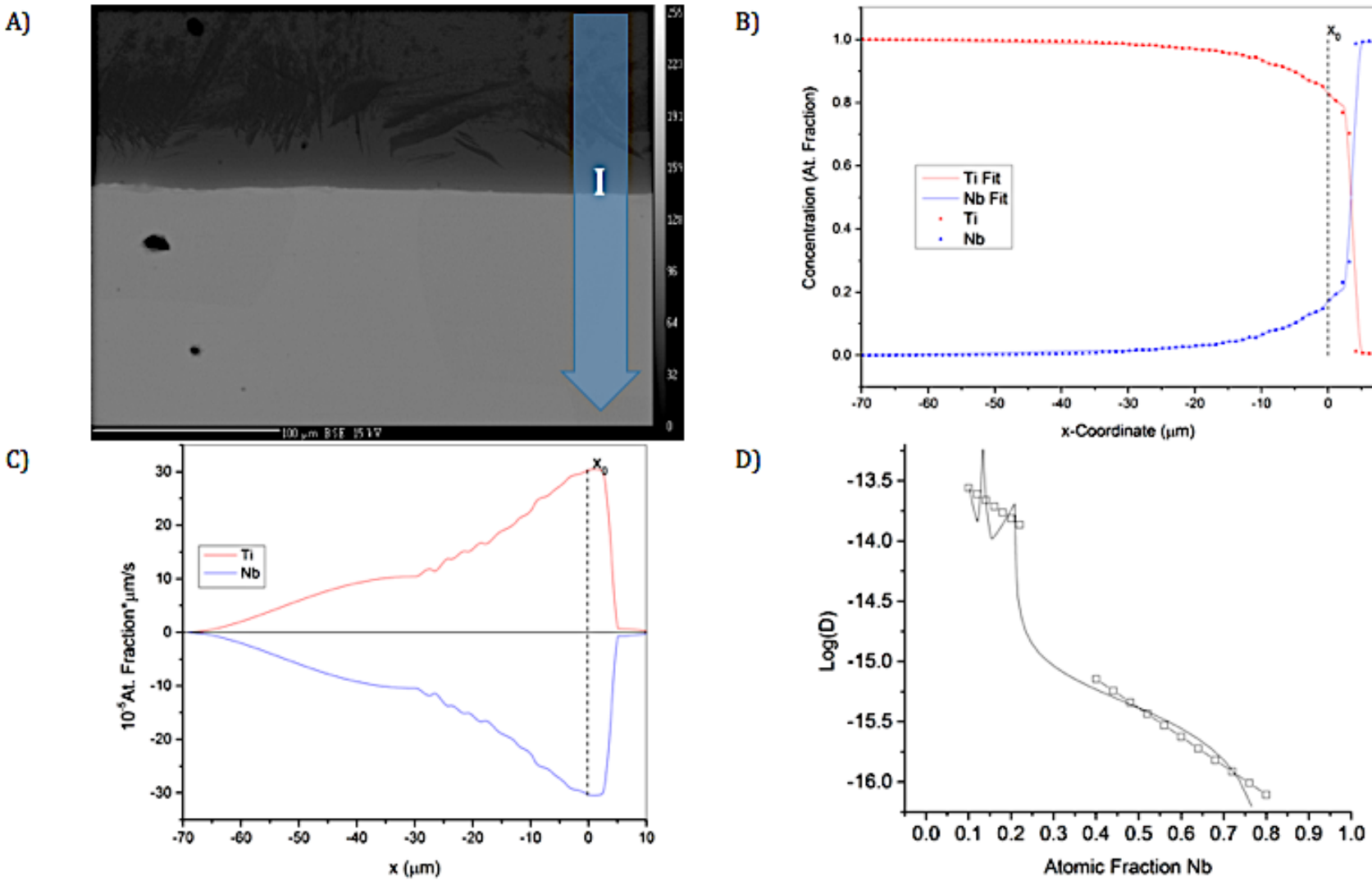

Figure 3.3: SPS-2 1000°C 80MPa Ti(+)-Nb(-) A) SEM BSE micrograph of interdiffusion interface, B) Concentration measurement from EPMA with *Multi*DiFlux fit overlapping, C) Interdiffusion flux calculated from *Multi*DiFlux, D) Interdiffusion coefficient calculated using Matano-Boltzmann method with linear approximations.

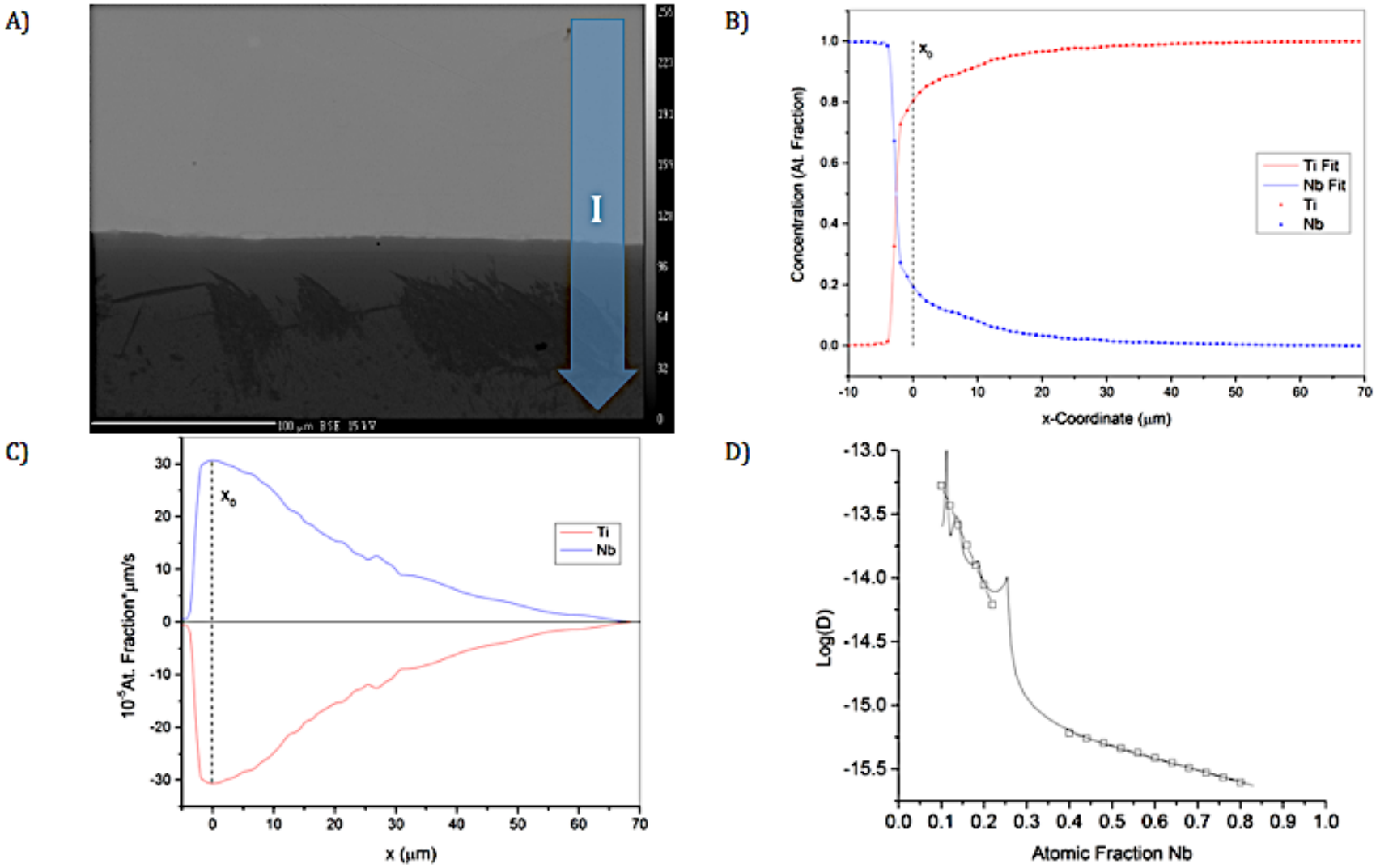

Figure 3.4: SPS-2 1000°C 80MPa Ti(-)-Nb(+) A) SEM BSE micrograph of interdiffusion interface, B) Concentration measurement from EPMA with *Multi*DiFlux fit overlapping, C) Interdiffusion flux calculated from *Multi*DiFlux, D) Interdiffusion coefficient calculated using Matano-Boltzmann method with linear approximations.

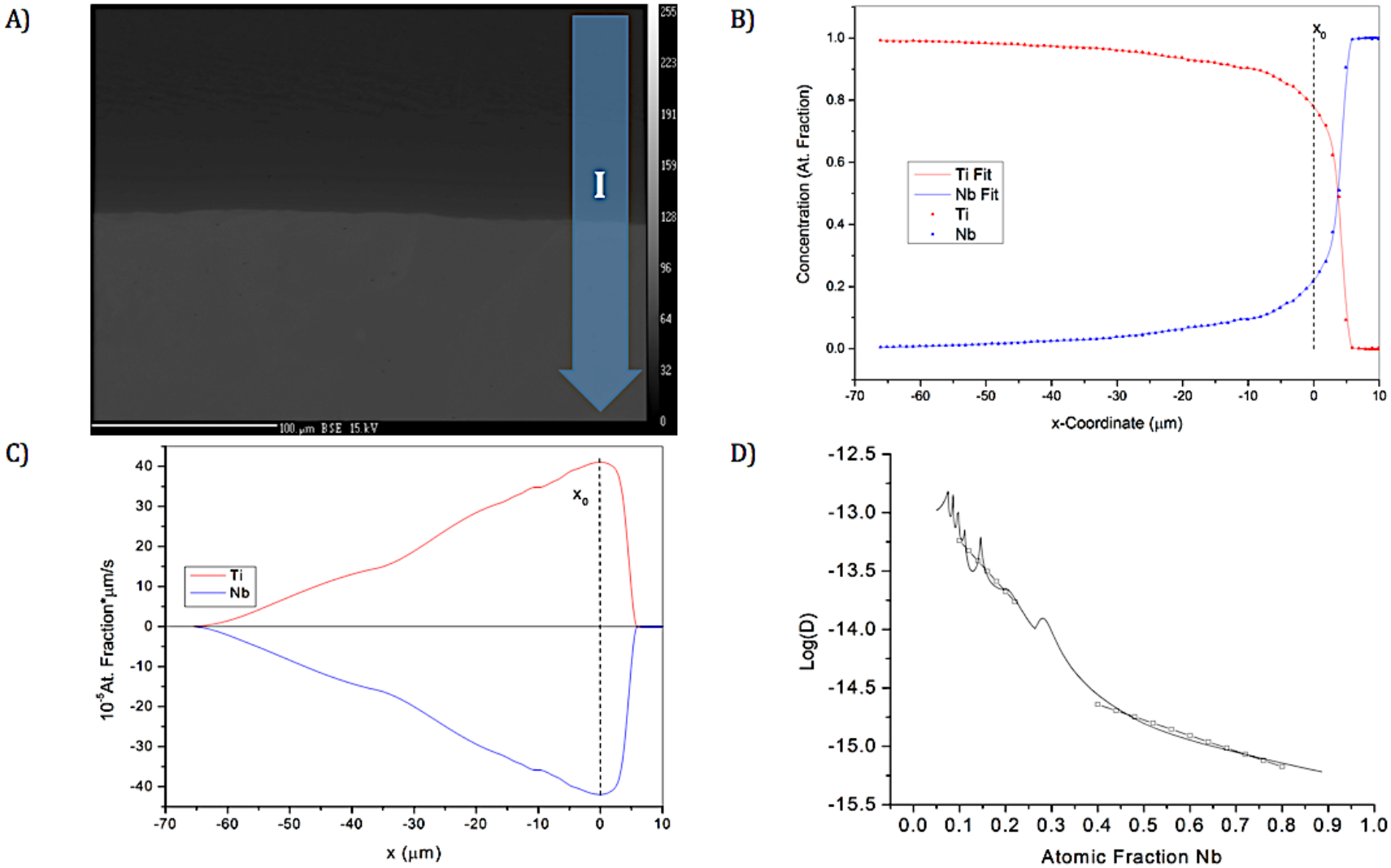

Figure 3.5: SPS-3, 1100°C 15MPa Ti(+)-Nb(-) A) SEM BSE micrograph of interdiffusion interface, B) Concentration measurement from EPMA with *Multi*DiFlux fit overlapping, C) Interdiffusion flux calculated from *Multi*DiFlux, D) Interdiffusion coefficient calculated using Matano-Boltzmann method with linear approximations.

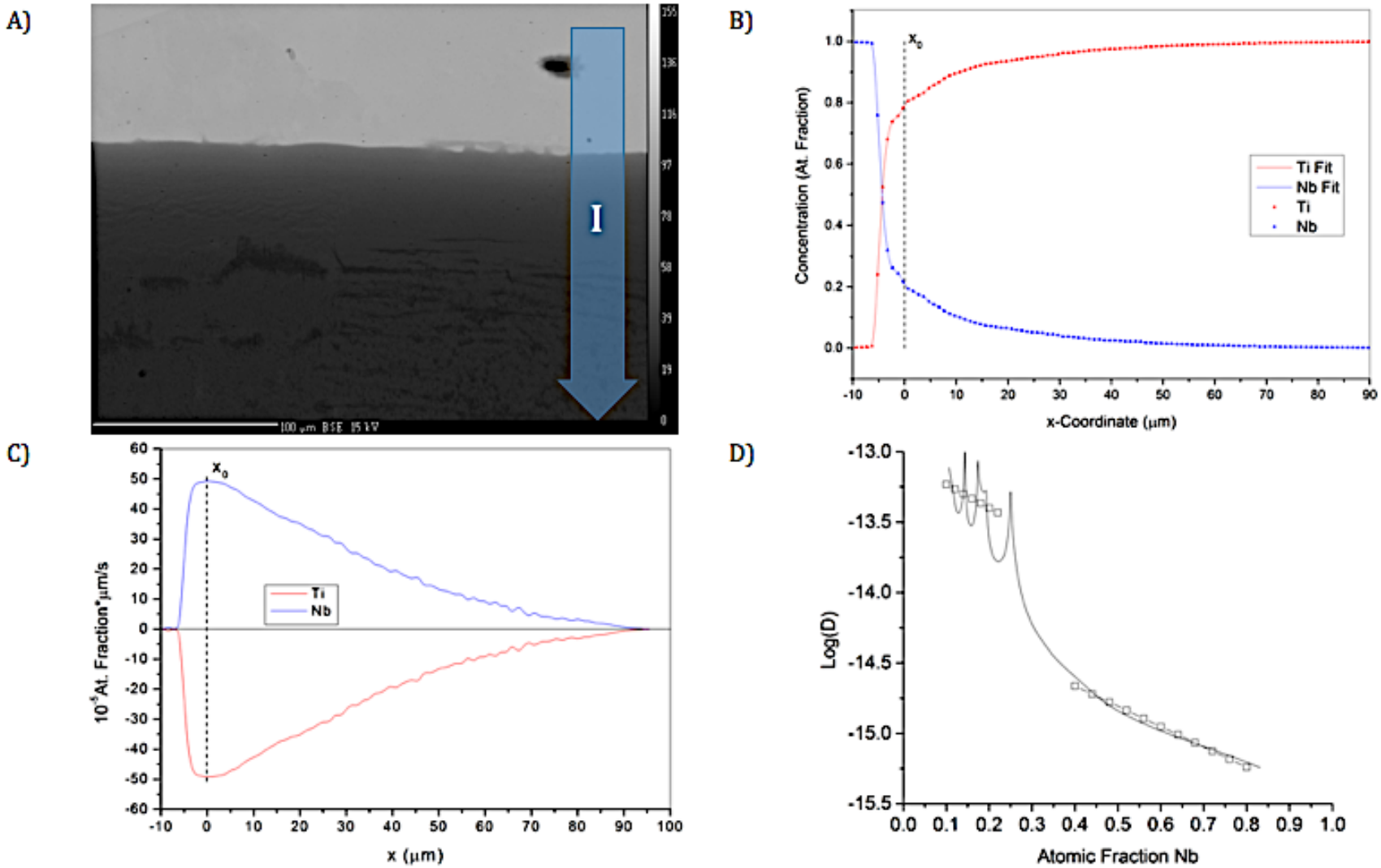

Figure 3.6: SPS-3, 1100°C 15MPa Ti(-)-Nb(+) A) SEM BSE micrograph of interdiffusion interface, B) Concentration measurement from EPMA with *Multi*DiFlux fit overlapping, C) Interdiffusion flux calculated from *Multi*DiFlux, D) Interdiffusion coefficient calculated using Matano-Boltzmann method with linear approximations.

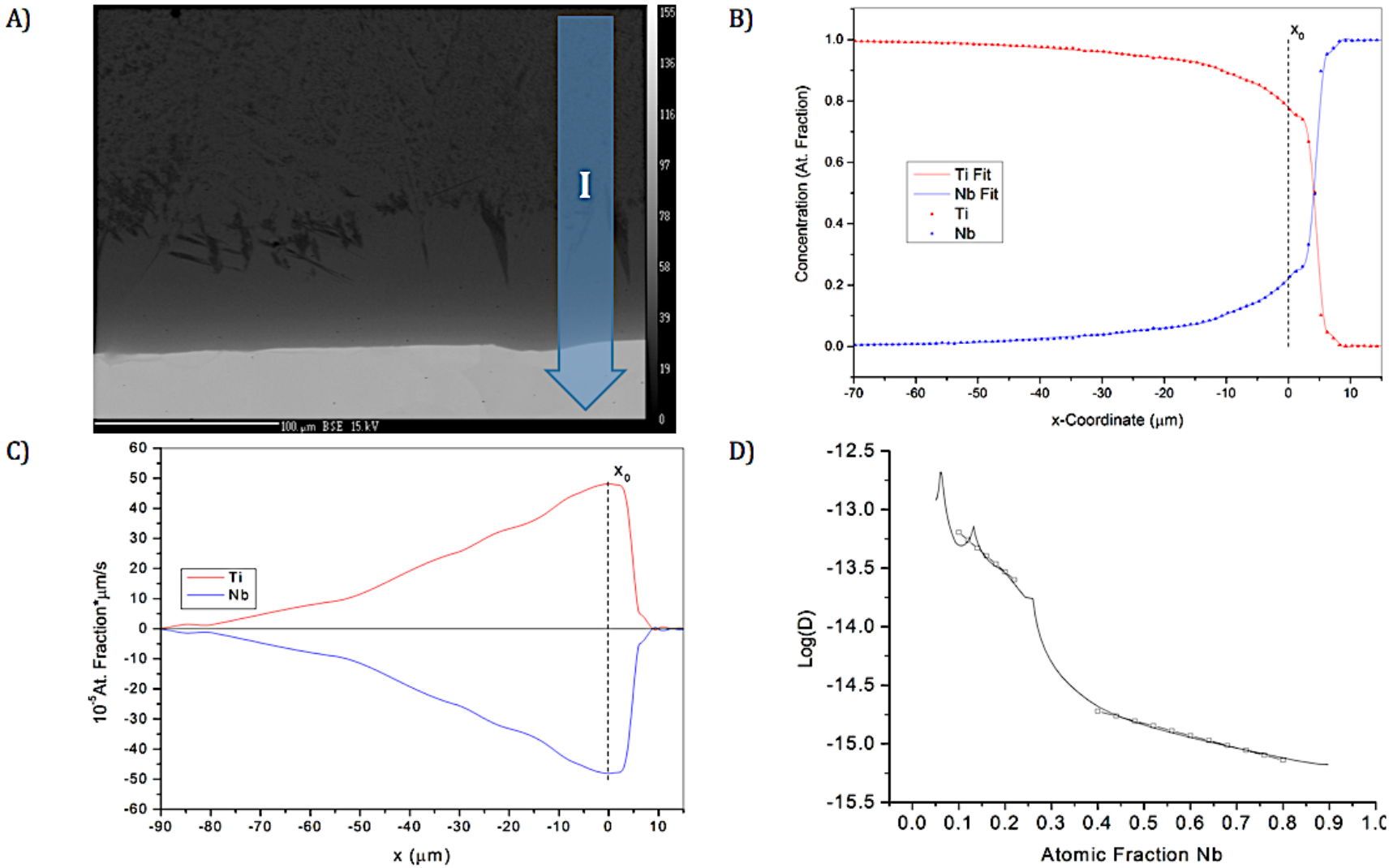

Figure 3.7: SPS-4, 1100°C 80MPa Ti(+)-Nb(-) A) SEM BSE micrograph of interdiffusion interface, B) Concentration measurement from EPMA with *Multi*DiFlux fit overlapping, C) Interdiffusion flux calculated from *Multi*DiFlux, D) Interdiffusion coefficient calculated using Matano-Boltzmann method with linear approximations.

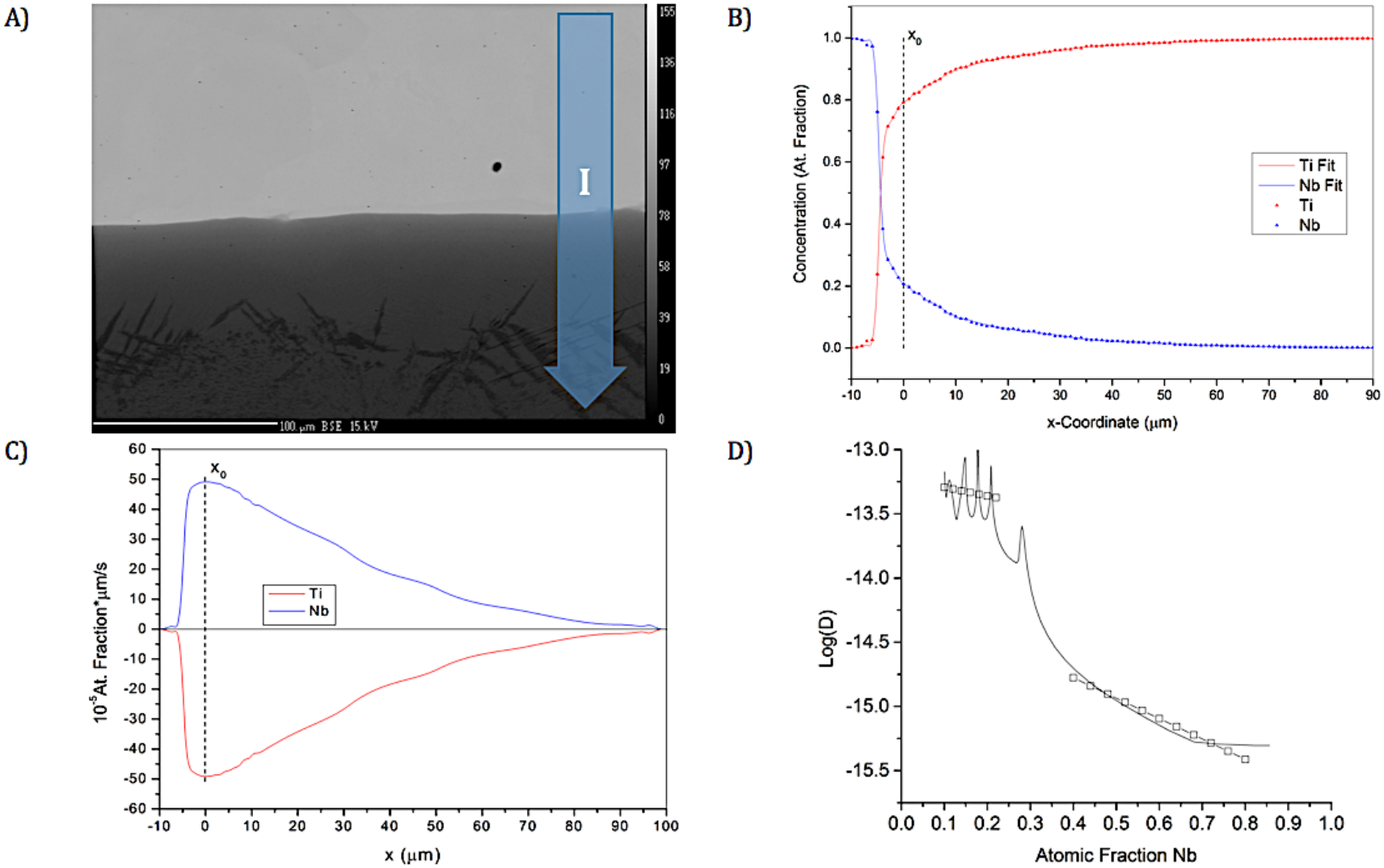

Figure 3.8: SPS-4, 1100°C 80MPa Ti(-)-Nb(+) A) SEM BSE micrograph of interdiffusion interface, B) Concentration measurement from EPMA with *Multi*DiFlux fit overlapping, C) Interdiffusion flux calculated from *Multi*DiFlux, D) Interdiffusion coefficient calculated using Matano-Boltzmann method with linear approximations.

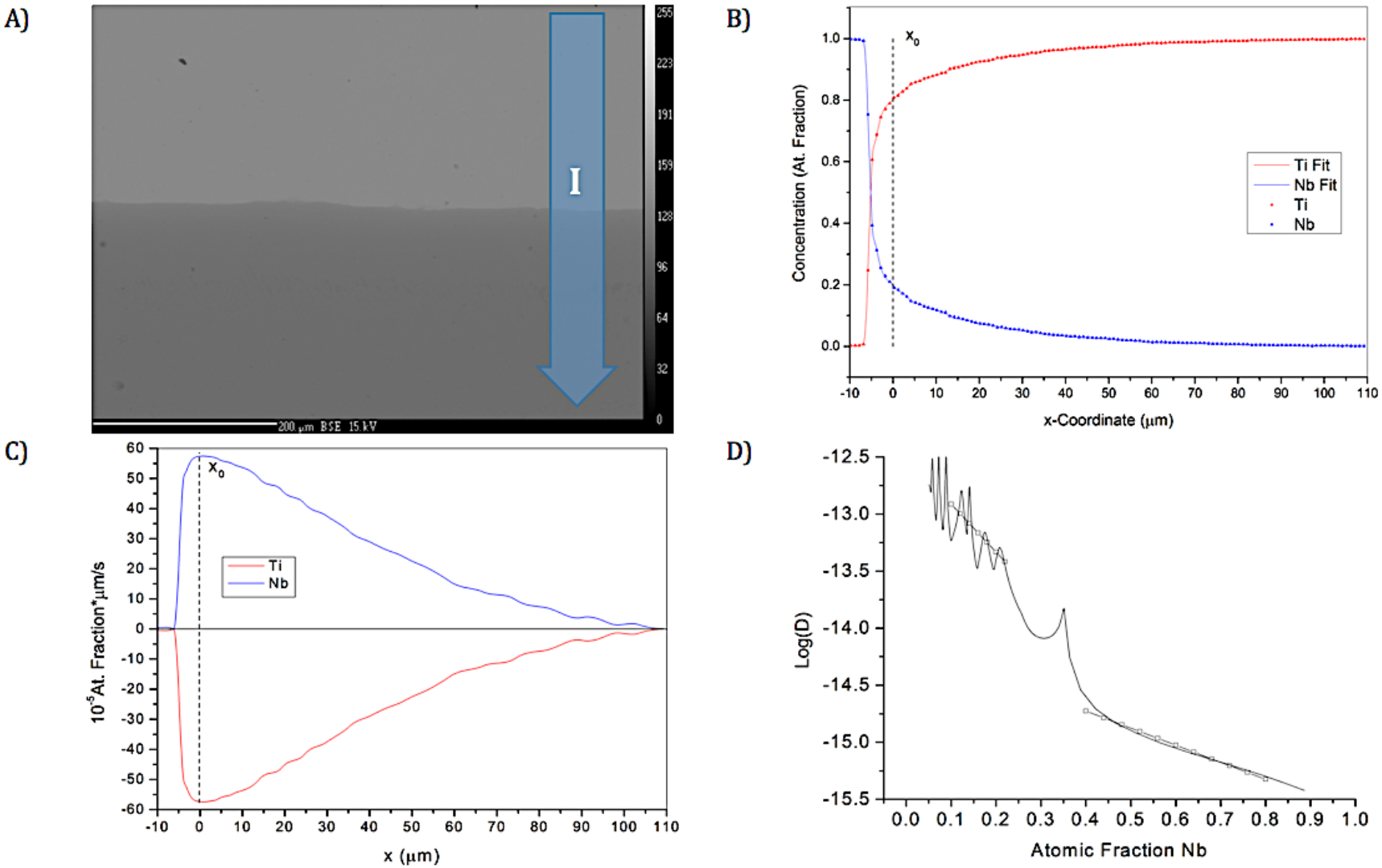

Figure 3.9: SPS-5, 1150°C 15MPa Ti(-)-Nb(+) A) SEM BSE micrograph of interdiffusion interface, B) Concentration measurement from EPMA with *Multi*DiFlux fit overlapping, C) Interdiffusion flux calculated from *Multi*DiFlux, D) Interdiffusion coefficient calculated using Matano-Boltzmann method with linear approximations.

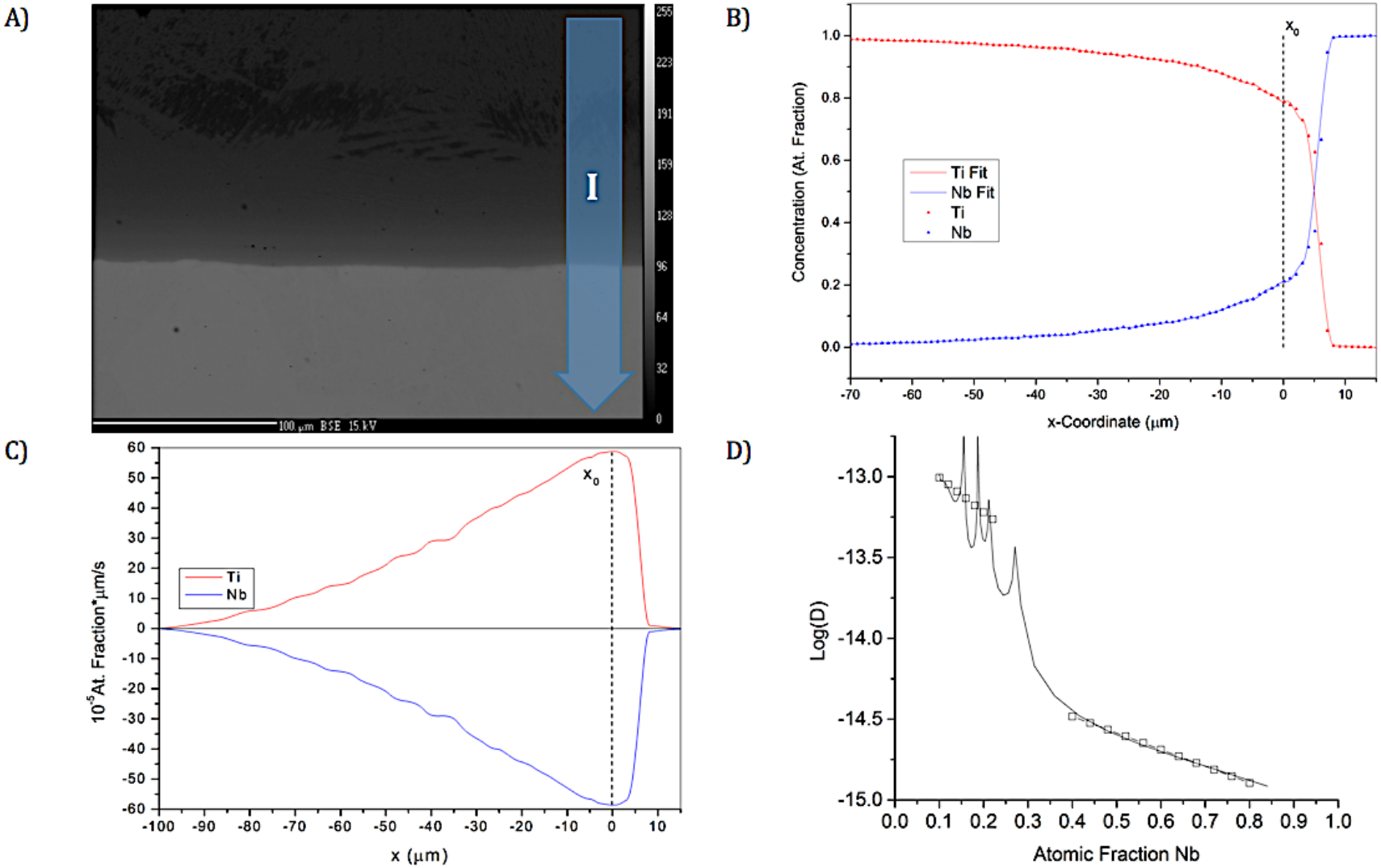

Figure 3.10: SPS-5, 1150°C 15MPa Ti(+)-Nb(-) A) SEM BSE micrograph of interdiffusion interface, B) Concentration measurement from EPMA with *Multi*DiFlux fit overlapping, C) Interdiffusion flux calculated from *Multi*DiFlux, D) Interdiffusion coefficient calculated using Matano-Boltzmann method with linear approximations.

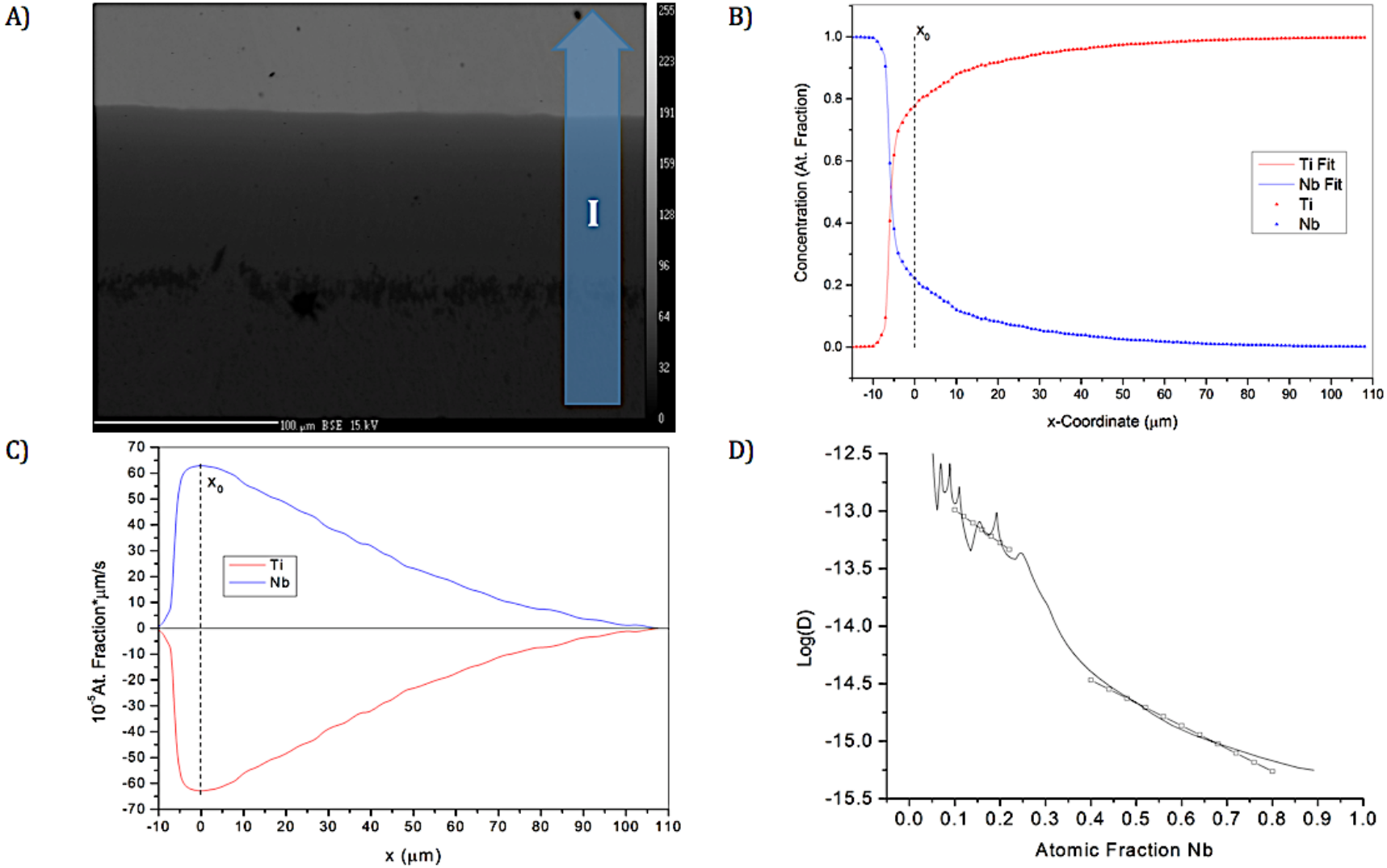

Figure 3.11: SPS-6, 1150°C 80MPa Ti(+)-Nb(-) A) SEM BSE micrograph of interdiffusion interface, B) Concentration measurement from EPMA with *Multi*DiFlux fit overlapping, C) Interdiffusion flux calculated from *Multi*DiFlux, D) Interdiffusion coefficient calculated using Matano-Boltzmann method with linear approximations.

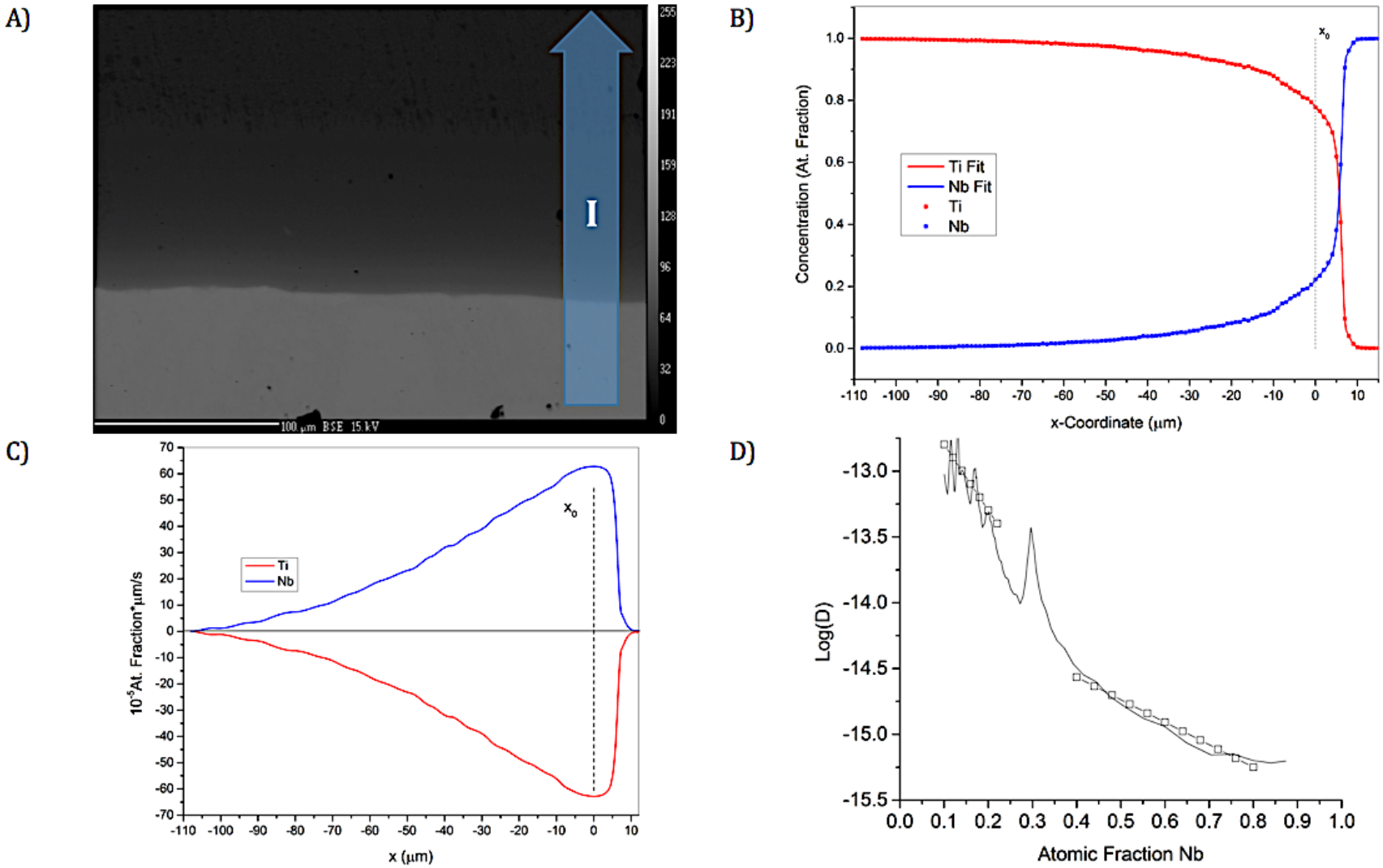

Figure 3.12: SPS-6, 1150°C 80MPa Ti(-)-Nb(+) A) SEM BSE micrograph of interdiffusion interface, B) Concentration measurement from EPMA with *Multi*DiFlux fit overlapping, C) Interdiffusion flux calculated from *Multi*DiFlux, D) Interdiffusion coefficient calculated using Matano-Boltzmann method with linear approximations.

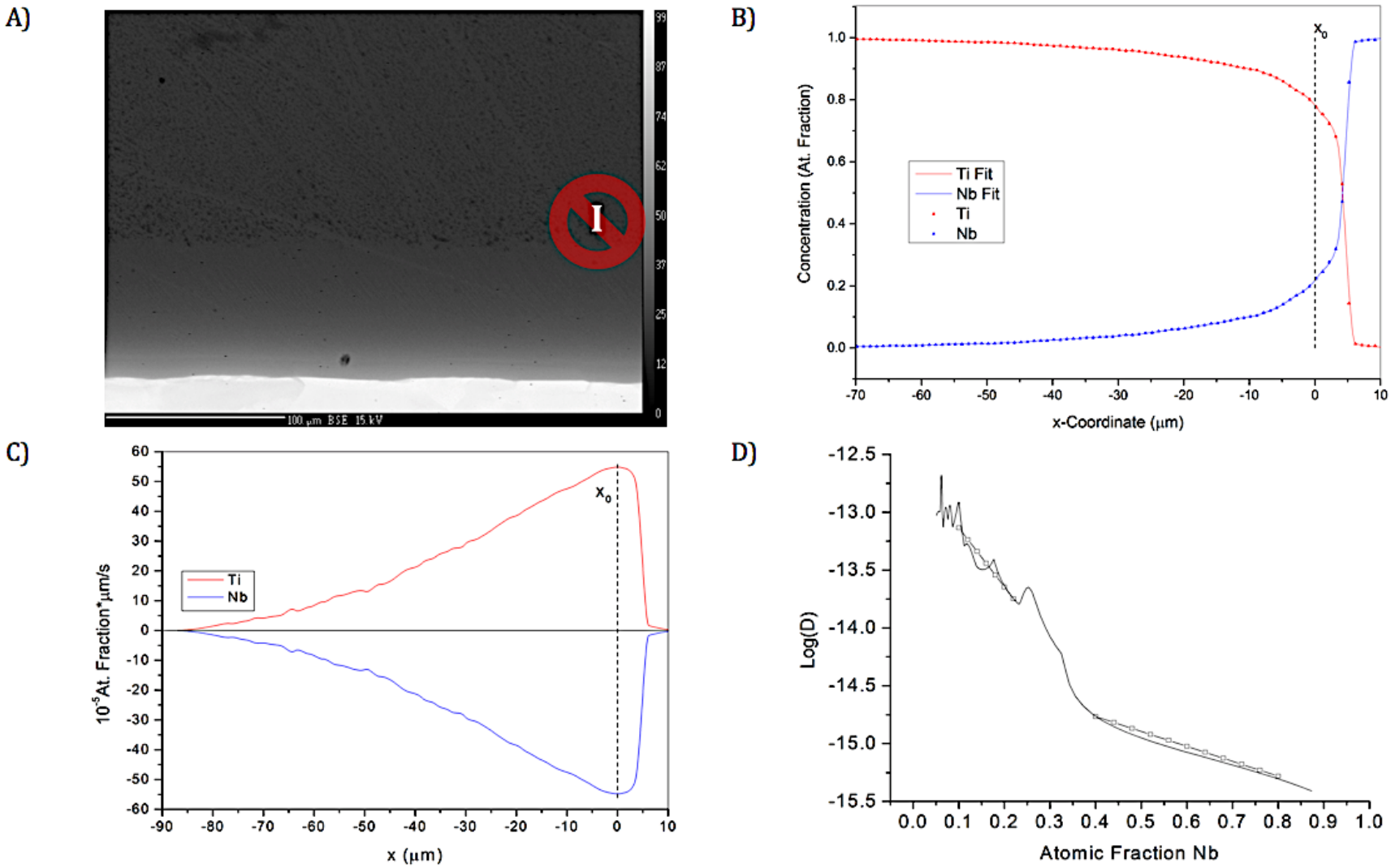

Figure 3.13: SPS-BN-1, 1100°C 15MPa A) SEM BSE micrograph of interdiffusion interface, B) Concentration measurement from EPMA with *Multi*DiFlux fit overlapping, C) Interdiffusion flux calculated from *Multi*DiFlux, D) Interdiffusion coefficient calculated using Matano-Boltzmann method with linear approximations.

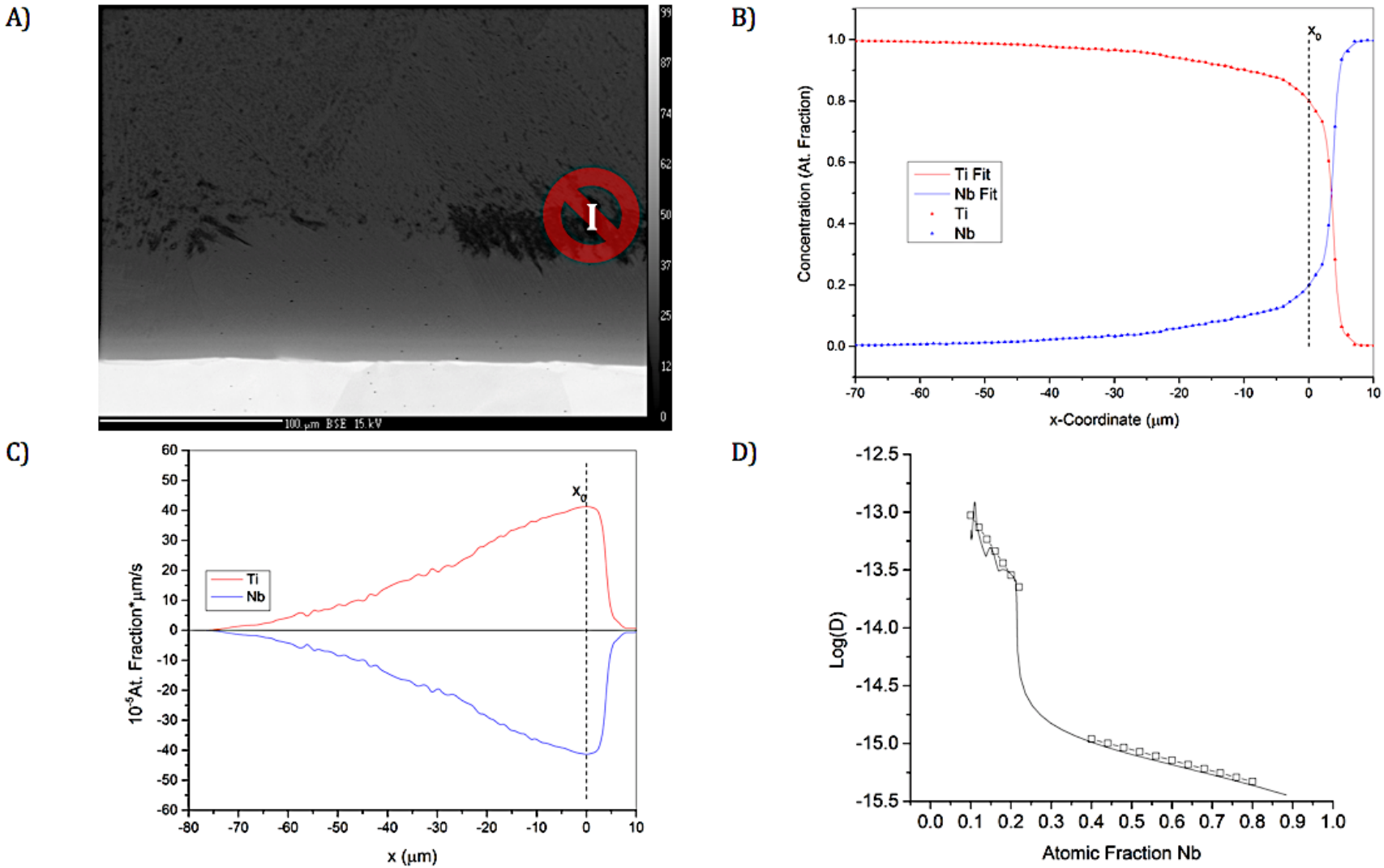

Figure 3.14: SPS-BN-2, 1100°C 80MPa A) SEM BSE micrograph of interdiffusion interface, B) Concentration measurement from EPMA with *Multi*DiFlux fit overlapping, C) Interdiffusion flux calculated from *Multi*DiFlux, D) Interdiffusion coefficient calculated using Matano-Boltzmann method with linear approximations.

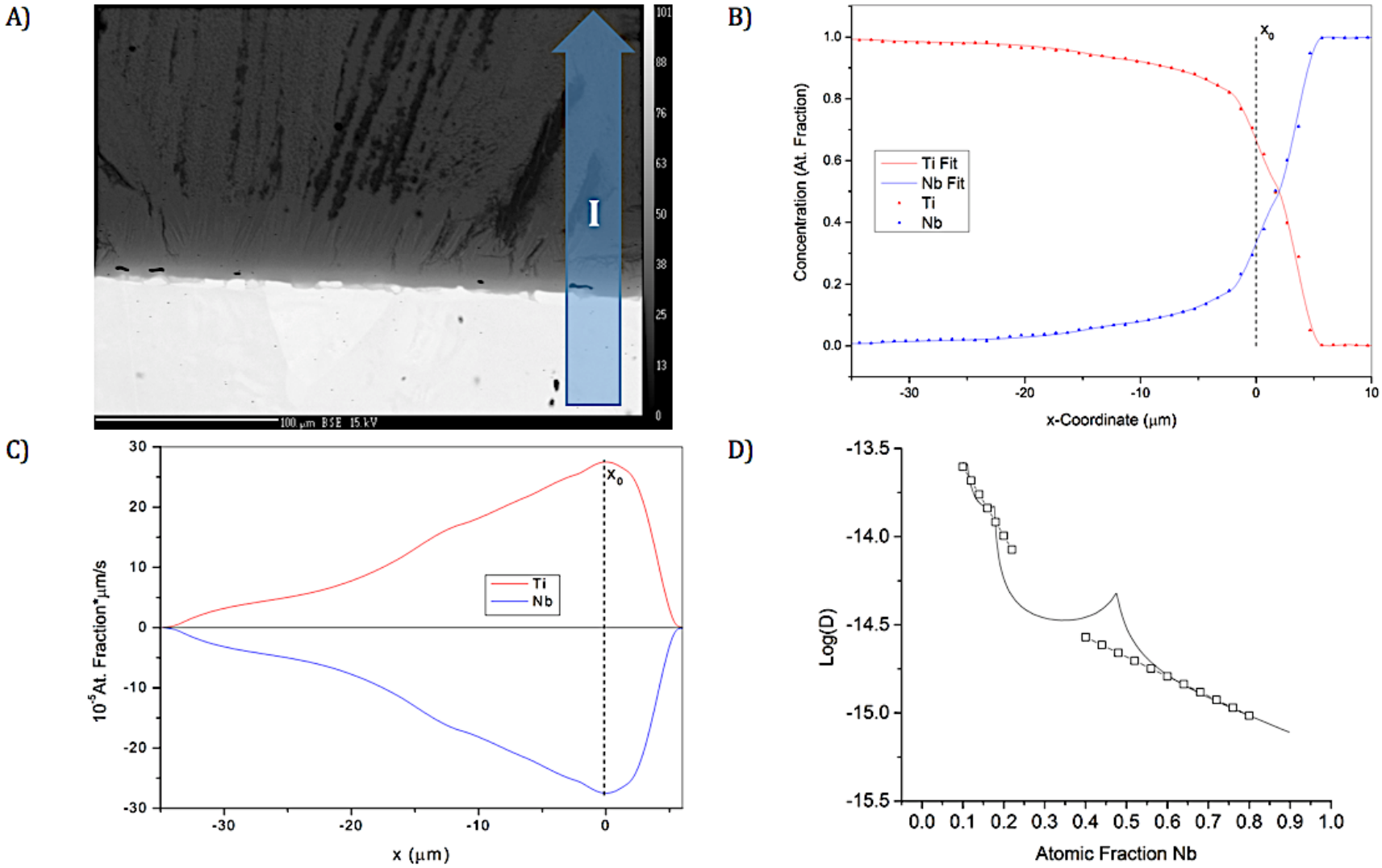

Figure 3.15: EMF-1, 1000°C Ti(-)-Nb(+) A) SEM BSE micrograph of interdiffusion interface, B) Concentration measurement from EPMA with *Multi*DiFlux fit overlapping, C) Interdiffusion flux calculated from *Multi*DiFlux, D) Interdiffusion coefficient calculated using Matano-Boltzmann method with linear approximations.

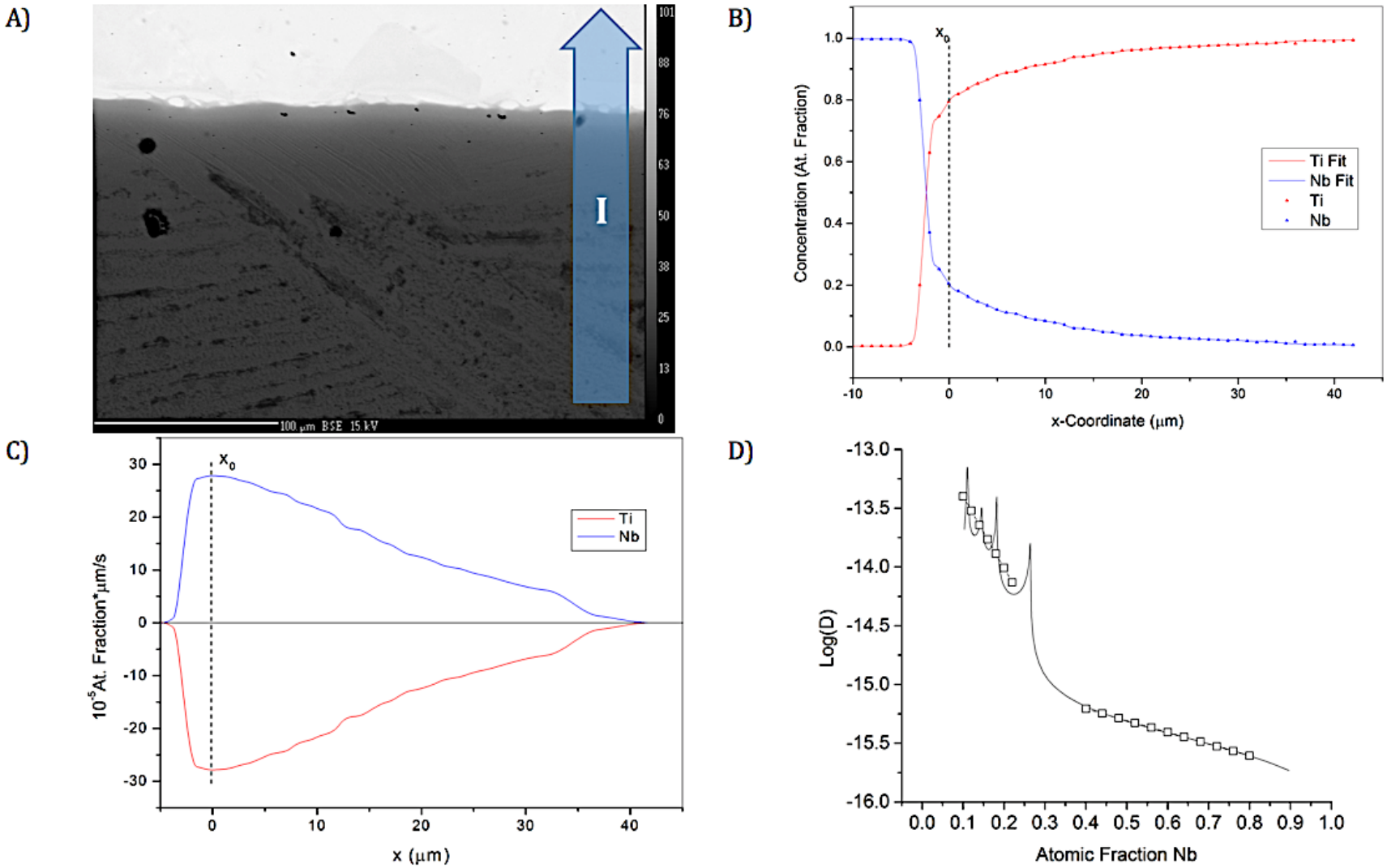

Figure 3.16: EMF-1, 1000°C Ti(+)-Nb(-) A) SEM BSE micrograph of interdiffusion interface, B) Concentration measurement from EPMA with *Multi*DiFlux fit overlapping, C) Interdiffusion flux calculated from *Multi*DiFlux, D) Interdiffusion coefficient calculated using Matano-Boltzmann method with linear approximations.

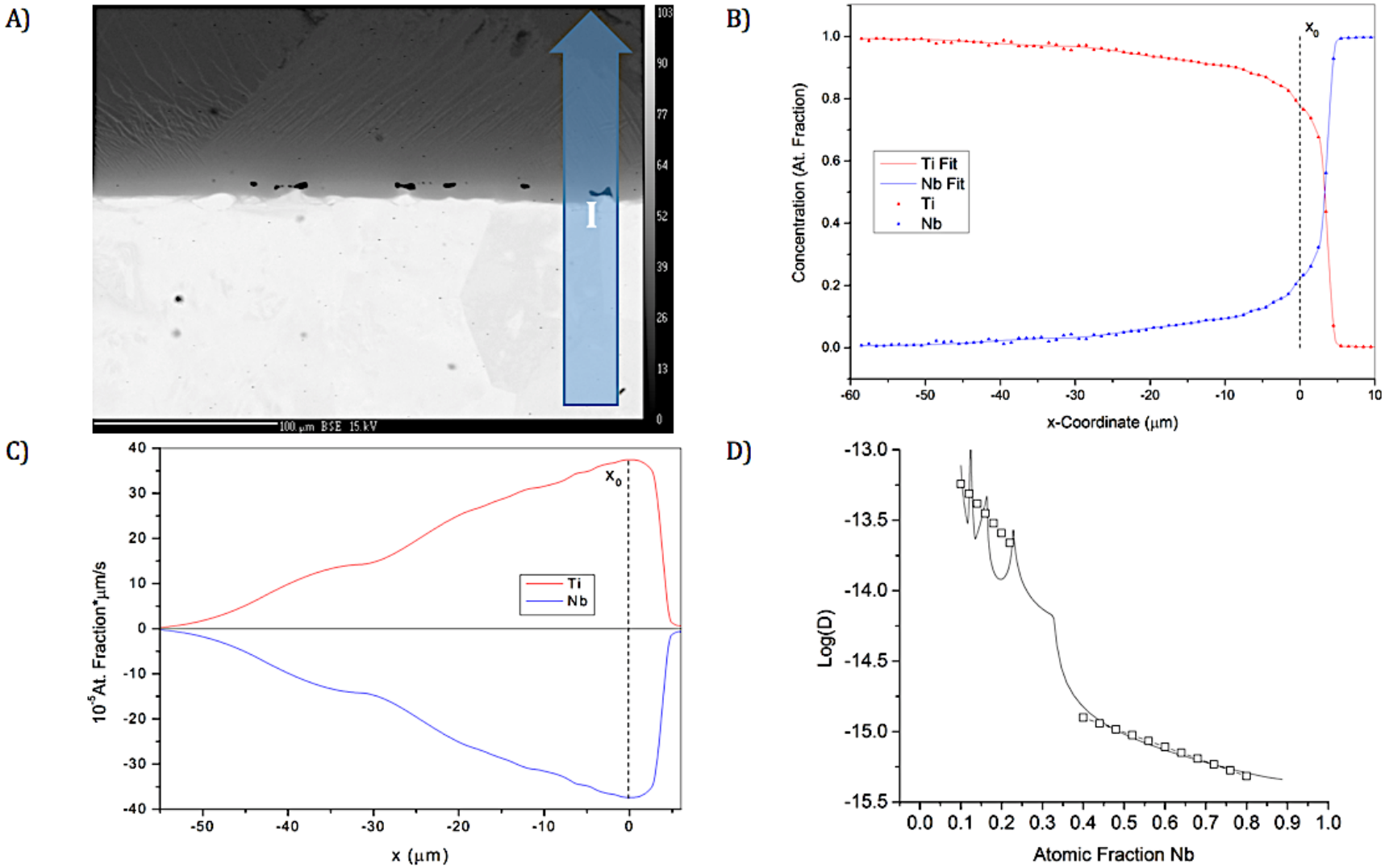

Figure 3.17: EMF-2, 1100°C Ti(-)-Nb(+) A) SEM BSE micrograph of interdiffusion interface, B) Concentration measurement from EPMA with *Multi*DiFlux fit overlapping, C) Interdiffusion flux calculated from *Multi*DiFlux, D) Interdiffusion coefficient calculated using Matano-Boltzmann method with linear approximations.

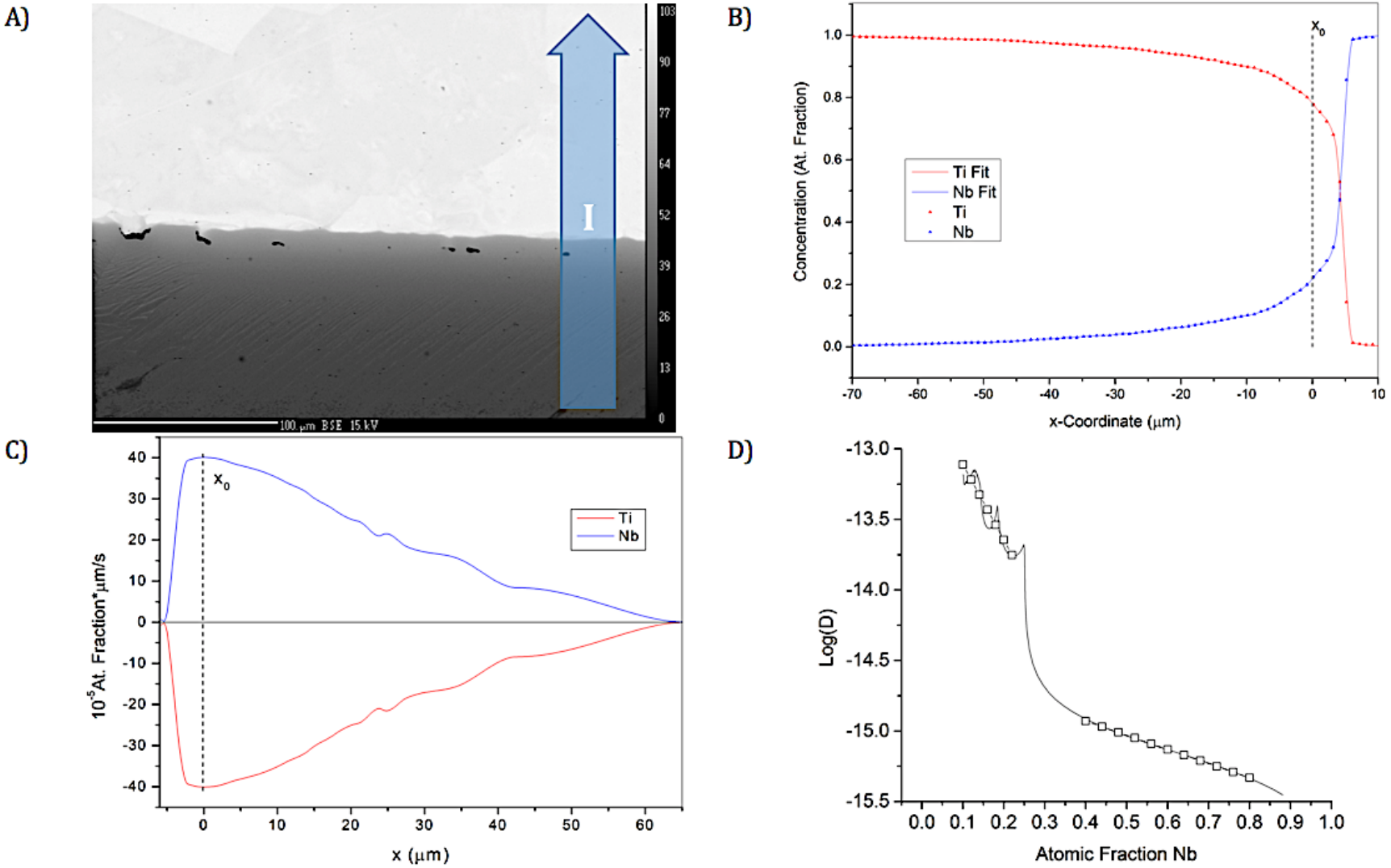

Figure 3.18: EMF-2, 1100°C Ti(+)-Nb(-) A) SEM BSE micrograph of interdiffusion interface, B) Concentration measurement from EPMA with *Multi*DiFlux fit overlapping, C) Interdiffusion flux calculated from *Multi*DiFlux, D) Interdiffusion coefficient calculated using Matano-Boltzmann method with linear approximations.

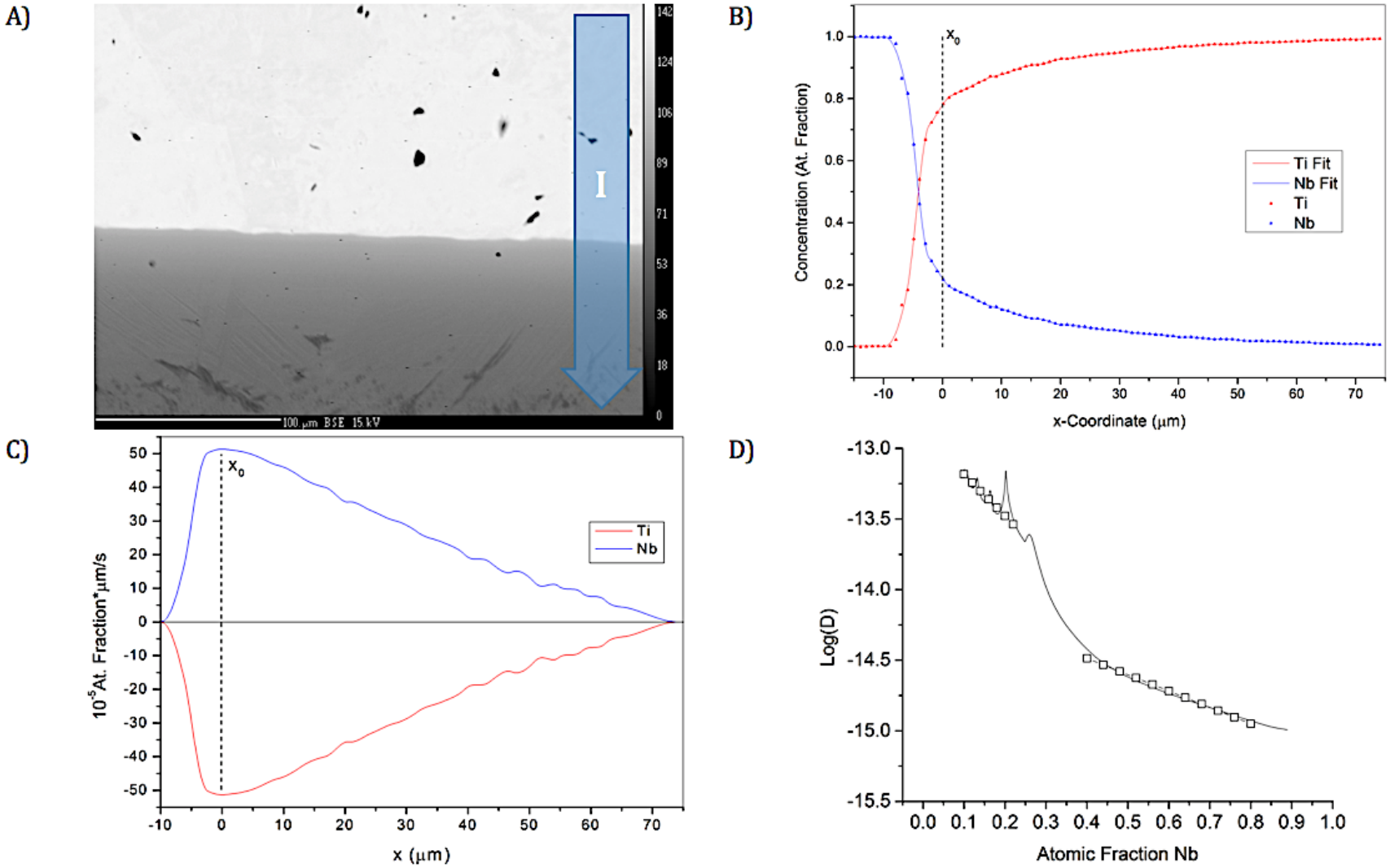

Figure 3.19: EMF-3, 1150°C Ti(-)-Nb(+) A) SEM BSE micrograph of interdiffusion interface, B) Concentration measurement from EPMA with *Multi*DiFlux fit overlapping, C) Interdiffusion flux calculated from *Multi*DiFlux, D) Interdiffusion coefficient calculated using Matano-Boltzmann method with linear approximations.

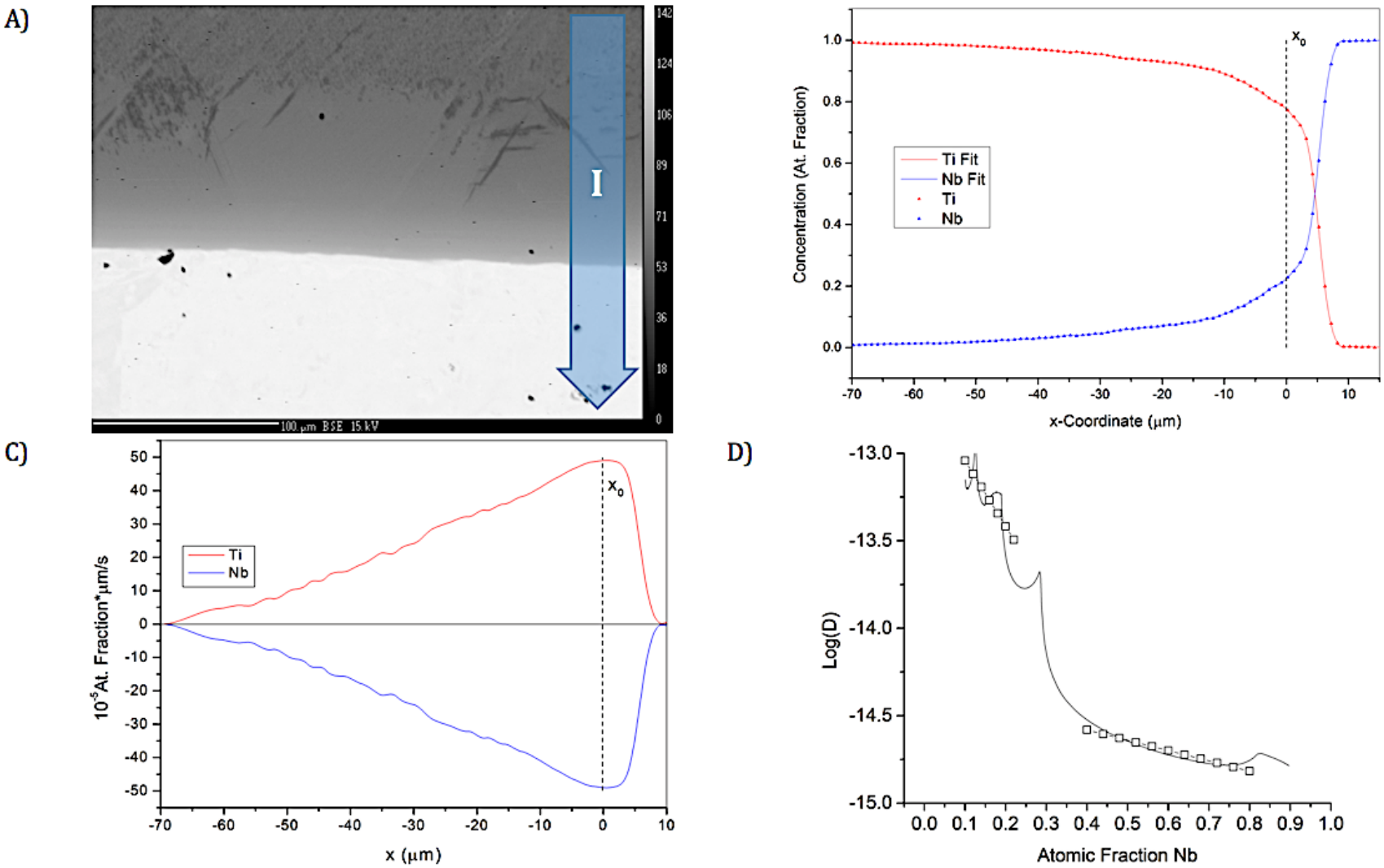

Figure 3.20: EMF-3, 1150°C Ti(+)-Nb(-) A) SEM BSE micrograph of interdiffusion interface, B) Concentration measurement from EPMA with *Multi*DiFlux fit overlapping, C) Interdiffusion flux calculated from *Multi*DiFlux, D) Interdiffusion coefficient calculated using Matano-Boltzmann method with linear approximations.

3.2 Data Analysis

This section compiles the how and why behind the data comparisons that have been made. For each temperature, there are three experiments which explore the change in diffusion according to pressure and current delivery. For activation energy to be studied a minimum of three temperatures is needed to find an average slope of the Arrhenius plot of ln(D) vs 1/T. Thus, activation energy plots, concentration dependence, can be made for both pressure sets 15MPa, 80MPa, and one for the constant DC in the EMF. Additionally, at 1100°C the influence of current was investigated by blocking the current flow through the diffusion couple in the SPS system. This is shown qualitatively by plotting the interdiffusion coefficient with and without current.

The experimental noise in the EPMA concentration measurements smoothed by *Multi*DiFlux develop large fluctuations in the interdiffusion coefficients, calculated using Equation 1, shown in Figures 3.1-3.20 D. linear approximations were made by taking raw data and calculating the linear fit over a specific concentration range. The resulting linear fit is shown overlaying the original interdiffusion coefficient data. The following compositions were used as linear approximation regions and will be referred to as low and high concentration Nb, 0.1 - 0.22 and 0.4 - 0.8 atomic fraction Nb. These regions are approximately linear in Ti-Nb literature [11][16]. Further calculations, such as activation energy, use the linear approximated data.

The activation energy was calculated by plotting the natural logarithm of the linear approximated interdiffusion coefficients $\ln(D[m^2s^{-1}])$ versus the inverse temperature $1/T$ K^{-1} the slope of this line was taken to equal $-Q/R$ where Q $kJmol^{-1}$ is the activation energy and R $kJmol^{-1}K^{-1}$ is the gas constant.

A note on possible errors. It is known from other authors that the sharp gradient at the Nb interface leads to measurement error in the high Nb concentration region at 1000 - 1150°C even for diffusion time of 2 days [35]. Hence, the one-hour hold time used in this study is a relatively short diffusion experiment which adds to the error in these measurements. The hold time was selected such that the experiments would have concentration gradient capable of being measured accurately with EPMA while not overheating the chamber of the SPS. The SPS is not often used for long duration high temperature experiments.

CHAPTER 4

Discussion

The effective interdiffusion data for Ti-Nb has not been reported on in literature regarding pulsed current with pressure in the SPS system. This data is useful for understanding the most influential effects on interdiffusion during sintering of beta phase powders. It is well known that the kinetic and diffusion behavior of a metallic system changes under SPS conditions. The Ti-Nb system is ideal for investigating the intrinsic effect of substitutional diffusion under SPS conditions since it forms a single phase solid solution and the vacancy mechanism is the main diffusional mode. In contrast, studies conducted with intermetallic systems have shown that kinetic barriers, nucleation, and growth, can be altered under SPS conditions depending on the material system in question. Hence, this study investigates the groundwork for multicomponent beta phase Ti-Nb-Al diffusion in the SPS system by considering changes in niobium, the interdiffusion rate limiting species. However, the information provided in the results section has shown that there is experimental error in the data which limits precise quantification.

4.1 Effects of Electromigration

Electromigration is a commonly referenced effect of SPS [8]. To study this effect during SPS the EMF was used at the same current density and temperature as the SPS. Since, the EMF is a constant DC, rather than a pulsed current, the electromigration flux in Equation 2 will likely have a slightly greater effect since the electric field E will be larger. To clarify, the SPS on-off pattern results in a duty cycle of 85.7% versus the EMF 100%. Figure 4.1 shows a comparison of the EMF and SPS interdiffusion coefficient for 1000, 1100°C at

varying current directions. The color variation shows the change in current direction at the diffusion interface. The red data set is current traveling from Ti to Nb and black is opposite. At 1000°C in the EMF the high concentration Nb shows a current directionality effect. However, the low concentration Nb at both 1000 and 1100°C shows a nominal change. At 1000°C, 15MPa in the SPS there is a relative decrease in the diffusion coefficient when the current travels from the Ti to Nb. Both 1000 and 1100°C in the SPS show some increase in the interdiffusion coefficient at low concentration Nb when current in from Nb to Ti. This is a similar effect to the Cu-Ni system wherein the current direction only had an effect when going from Ni to Cu [31]. At 1100°C in EMF and SPS, the current density is mostly insufficient to cause electron wind effects at high concentration Nb. From the comparison of the current direction in EMF and SPS at lower temperatures the current direction may play a role in effecting the interdiffusion coefficient. However, at higher temperatures, this effect is lessened.

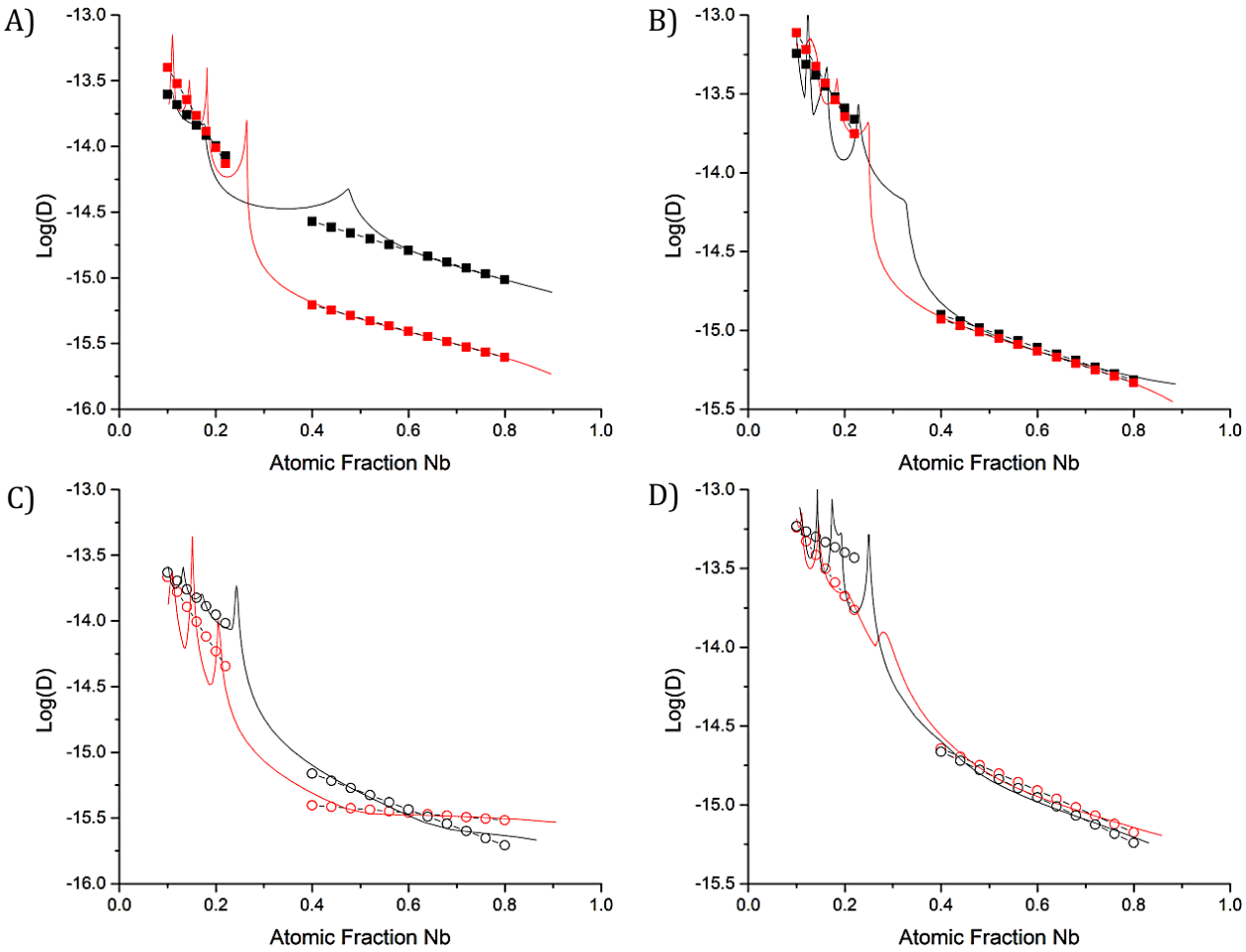

Figure 4.1: Electric current polarity comparison of interdiffusion coefficients at the following temperatures, red is Ti(-)-Nb(+), black is Ti(+)-Nb(-) A) EMF-1 1000°C, B) EMF-2 1100°C, C) SPS-1 1000°C, D) SPS-3 1100°C

4.2 Effects of SPS with Pressure and Without Current

To block the current in the SPS boron nitride inserts where placed around the diffusion couple. These two experiments at 1100°C, with pressures 15MPa and 80MPa, investigate both the role of current on diffusion in the SPS and the effect of increased pressure without current. Figure 4.2 provides a comparison of 1100°C with and without current at 15MPa and 80MPa. The current polarity has been kept constant for this comparison. Surprisingly, at low concentration Nb and 15MPa, the interdiffusion coefficient

is larger without current. Possible influences on this result could be from the fitting procedure used by *Multi*DiFlux, the linear approximation made from the composition profile, and the measurement itself. The experimental noise can be seen in Figures 3.5, 3.7, 3.13, 3.14 section D. However, at 15 and 80MPa high concentration Nb show a decrease in diffusion from the absence of current. It is expected that the interdiffusion coefficient should be found closer to the literature values after removing the current if the sample is at the same temperature. Table 2.1 highlights that both experiments with boron nitride encountered experimental issues with the thermocouple which may have added to the errors previously mentioned. It can be concluded that the presence of compounding errors is likely at fault for the increase of the diffusion coefficient at low concentration Nb in the SPS at 15 and 80MPa.

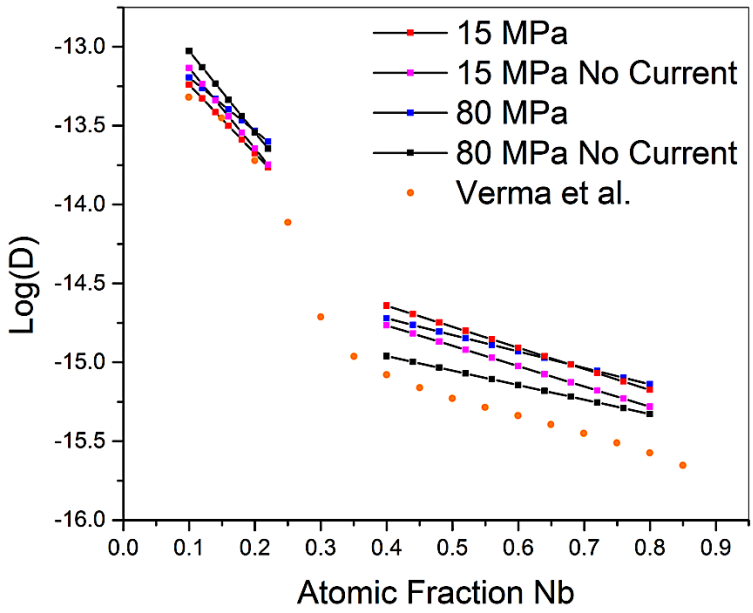

Figure 4.2: Interdiffusion coefficient for SPS samples at 1100°C with and without current

The hydrostatic pressure increases from 15 to 80MPa without the influence of current should decrease the diffusion coefficient on the basis of Equation 4. As expected this

decrease is seen most notably in the 80MPa sample at high Nb concentration. Had the interdiffusion of both 15 and 80MPa samples with current blocked been decreased compared to the other experiments at 1100°C a definitive stress state, either hydrostatic or deviatoric, would be concluded, but this is not the case.

4.3 Effects of SPS parameters on Interdiffusion

The effects of combined temperature via current and pressure has been investigated for Ti-Nb. Figure 4.3 shows the change in interdiffusion coefficient calculated using the Matano Boltzmann method with increasing sample pressure in the SPS. The discussion of these effects is broken into two sections for the low and high concentration Nb. The SPS data is compared to the Ti-Nb interdiffusion coefficients found by Verma et al. at 1100 and 1150°C [16]. Prasad et al. also studied the Ti-Nb system but did not report on the high concentration niobium because of the large amounts of error found in measuring the steep Nb gradient [35]. As previously mentioned, this is due to sluggish Nb diffusion, and shortened annealing times exacerbate this error. It is worth noting that the work by Verma is consistent with the low concentration Nb work from Prasad et al.

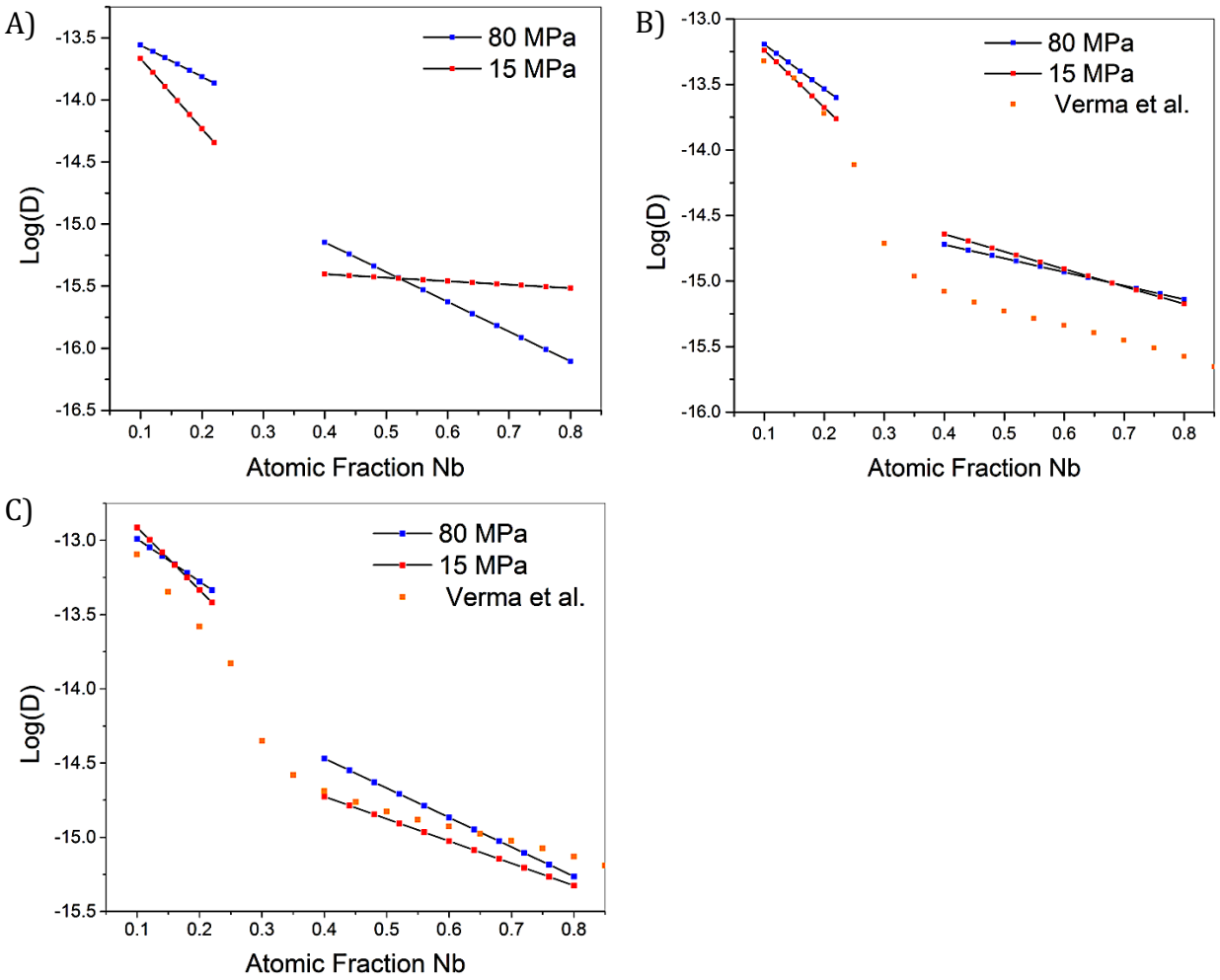

Figure 4.3: SPS (Pressure and Current) composition dependent interdiffusion coefficients at the following temperatures A) 1000°C; SPS-1, SPS-2 B) 1100°C; SPS-3, SPS-4, C) 1150°C; SPS-5, SPS-6

In Figure 4.3 the low concentration Nb at 1000 and 1100°C shows an increase in diffusion coefficient with increased pressure, whereas the 1150°C sample shows little to no change from pressure. Note that in Table 3.1 the current density and temperature has stayed nominally the same for all experiments with the same set temperature. It can be ruled out that a temperature variation has caused this trend. To explain this result pressure must be considered as either hydrostatic or deviatoric. From Equation 5 it is clear the hydrostatic component of the applied stress would result in a decrease in the interdiffusion

coefficient which is not completely evident from the data shown. Deviatoric, stress on the other hand, increases the flux from Equation 8. Hence, it is presumed that deviatoric stresses are responsible for the increased diffusion. Yet, the experiments in the SPS with current blocked showed evidence of hydrostatic behavior.

The effect of pressure on high concentration Nb is very notable at 1000°C but lessens with increased temperature. Also, at 1150°C the diffusion coefficient is essentially the same for either pressure and is in close agreement with literature. The increase in diffusion from current and pressure at 1150°C is negligible at high concentration Nb.

The effects of current plus pressure in other systems has shown increased vacancy formation and enhanced defect mobility [36][33]. A conclusion can be drawn that enhanced diffusion in the SPS is from current, and pressure enhances this effect. An important point is that the current and pressure effects are reduced as temperature increases.

The greatest effect on the interdiffusion coefficient from SPS is at low temperature and low concentration of Nb. The sensitivity to lower concentration Nb and lower temperatures shed light on this complex enhancement of diffusion.

To further the analysis of the low concentration Nb the activation energy for diffusion is compared between the SPS at 15 and 80MPa, EMF (current only), and Verma's work [16]. Figure 4.4 shows activation energy from applying current plus pressure, current alone, and standard diffusion experiments without either current or pressure. The largest drop in activation energy was found from the EMF. This result is likely due to two factors. First, the application of a constant DC rather than pulsed. Which slightly increases the amount of electrical energy in the sample. Second, the absence of hydrostatic pressure in

the EMF which would decrease the diffusion coefficient. The SPS data at 15 and 80MPa show that the activation energy can be lowered with increasing the pressure applied. The average decrease in activation energy from EMF is 105kJmol^{-1} while the application of pressure in the SPS resulted in an average decrease of 38 and 70kJmol^{-1} for 15 and 80MPa respectively.

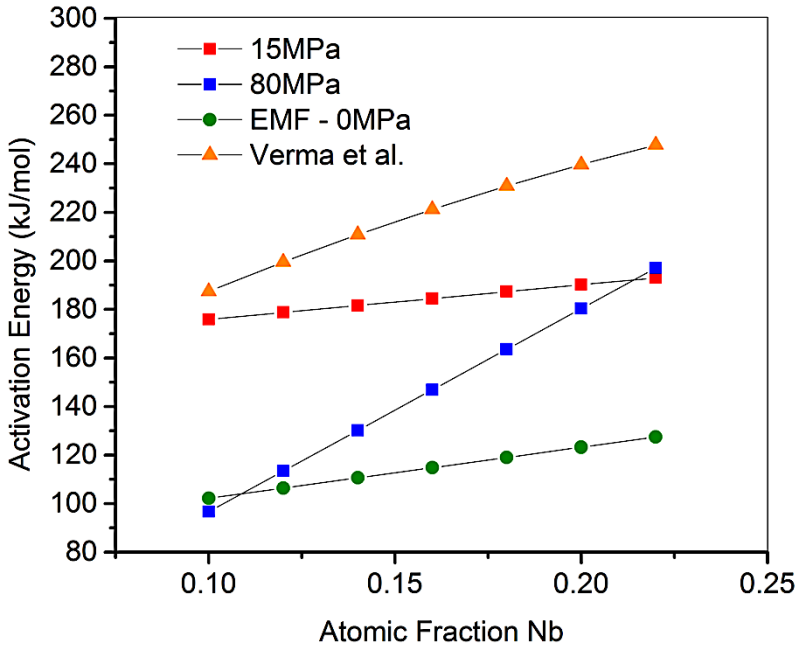

Figure 4.4: Activation energy of low concentration, 0.1-0.22 atomic fraction Nb, of SPS, EMF (no pressure), and Verma et al. [16].

CHAPTER 5

Conclusion

5.1 Summary of Findings

This summary is written in order of the least to most effecting parameters on interdiffusion of the Ti-Nb system regarding current and pressure. The investigated effects are as follows; current direction, pressure with and without current, and combined pressure plus current.

Electromigration, also known as the electron wind effect, is a commonly mentioned effect of the SPS. The electron wind presence shows a small effect at 1000°C in the SPS and lessens with increased temperature. This is consistent with the results from the EMF experiments. The resulting effects of current namely increased vacancy formation, and increased defect mobility are the likely contributors to the enhanced electron wind diffusion seen in the EMF study. Furthermore, the constant DC current caused an increase in these effects due to the increase in overall power from the 100% duty cycle.

Pressure with and without current was studied in the SPS and EMF systems by means of blocking the current and applying effectively no pressure in the EMF system. The goal of investigating pressure was to measure the influence pressure has on interdiffusion in the SPS. The application of pressure in the SPS is common due to its beneficial effects on densifying powders. Complex stress states can be split into two components deviatoric and hydrostatic. Deviatoric stress aids diffusion while hydrostatic hinders diffusion. The Hydrostatic mechanism appears to be taking place in the SPS without current with the increase of pressure. However, with current applied, the increase of pressure increases the diffusion coefficient. This leads to a conflicting result in terms of determining the pressure

state being hydrostatic or deviatoric. It is found that within the 15 to 80MPa stress range the interdiffusion is increased, but the mechanism is not fully clear.

The SPS system uses pressure and current simultaneously to densify powdered materials. The combined effects of pressure and current on the interdiffusion of Ti-Nb have shown the increase in diffusion coefficient with increasing pressure. Also, changes in diffusion with current and pressure are dependent on the concentration. However, there is limited precision in the high concentration of Nb due to several factors including the sluggish diffusion and short experimental annealing times. At low concentration Nb, the addition of pressure from 15 to 80MPa increases the effect of current by lowering the activation energy by 32kJmol^{-1}. The well-established effects from current are increased vacancy concentration and increased defect mobility, yet the mechanism for decreasing activation energy with pressure is not fully understood. In summary, the effects of current plus pressure have been identified and their relative magnitudes examined.

5.2 Directions for Future Work

The following is a short summary of potential work to advance the goal of accurately modeling Ti-Nb-Al interdiffusion in the SPS. Experiments in the ternary phase should be done after considering the following aspects; method of interdiffusion coefficient calculation, use of Kirkendall markers, and limiting experimental errors. A final suggestion is made for using the SPS as a processing step for bonding diffusion couples.

Modeling of multicomponent powder system to full homogenization will require mobility parameters which are derived from interdiffusion coefficients. To determine the interdiffusion coefficients for a ternary system experiments should be designed to take

advantage of the following diffusion analysis methods Dayananda-Sohn, Boltzmann-Matano, Whittle-Green, or the pseudobinary approach conducting experiments with and without current. However, there are limitations to each of these methods which may make an interdiffusion study in the SPS or EMF difficult. Other methods which make use of Kirkendall plane should be explored as they may lessen the necessary amount of experiments. However, the study of multicomponent diffusion is still developing, so there may be other methods that arise as time moves forward.

Fiducial markers are used to identify the Kirkendall plane. Yet, the selection of the fiducial marker material can be a difficult. Stable ceramic oxides make good fiducial markers since they do not play a role in diffusion during annealing. Thorium oxide is often used because of its inertness, although its radioactive behavior is a safety issue. Other methods and advanced techniques that make use of Kirkendall markers can be found in Aloke Paul's book "*Thermodynamics, Diffusion and The Kirkendall Effect in Solids*." [17].

Uncertainty in experimental data causes difficulty in determining the exact changes from current polarity, and current plus pressure. Additionally, sluggish diffusion of niobium makes the concentration gradient very sharp especially at low homologous temperature and short diffusion time. To decrease these error the following ideas are suggested.

- Increase annealing time in the SPS and EMF
- Determine changes in mechanical properties at desired temperature with current and pressure
- Confirm uniform temperature and current flux by modelling the experimental configuration

- Control the diffusion interface stress state, either hydrostatic or deviatoric

Since the SPS is not designed for very long hold times one solution is to conduct SPS-like experiments in the EMF. The EMF would need to be modified to pulse the electric current and a pressure sensor should be added to ensure correct sample pressure. With these modifications the experimental time could be drastically increased.

A brief note on using SPS to quickly bond diffusion couples. Bonding materials in the SPS allows for fast production of several diffusion couple in a single sample. Some of the advantages of SPS diffusion bonding have been reported by authors in respect to Ti-Ni which found the lack of pores and mechanical properties is superior to furnace heated bonding [37]. Prior to bonding Kirkendall markers can be added to the interface. The result is a well bonded diffusion couple with desired initial composition, and Kirkendall markers at the interface which can be cut into smaller specimen using an EDM. Furthermore, by using minimal time, low pressure and temperature the bond has very little diffusional interaction. The small diffusion interaction at the bond can be considered negligible based on two factors. First and most importantly, temperature for diffusion bonding should be hundreds of degrees lower than the diffusion annealing temperature. Temperature has an exponential effect on diffusion so the diffusion from bonding is small. Secondly, only a few minutes at bonding temperature is necessary. Hence, SPS diffusion bonding should have negligible impact on a typical diffusion experiment at high homologous temperature for several hours resulting in insignificant change of boundary conditions. Overall, SPS bonding provides an efficient way to make diffusion couples.

REFERENCES

[1] A. K. Sachdev, K. Kulkarni, Z. Z. Fang, R. Yang, and V. Girshov, "Titanium for Automotive Applications: Challenges and Opportunities in Materials and Processing," *Jom*, vol. 64, no. 5, pp. 553–565, 2012.

[2] S. Seong, O. Younossi, B. Goldsmith, T. Lang, and M. Neumann, *Titanium: Industrial Base, Price Trends, and Technology Initiatives*. RAND Corporation, 2009.

[3] K. Kothari, R. Radhakrishnan, and N. M. Wereley, "Advances in gamma titanium aluminides and their manufacturing techniques," *Prog. Aerosp. Sci.*, vol. 55, pp. 1–16, Nov. 2012.

[4] J. Withers, J. Laughlin, Y. Elkadi, J. DeSilva, and R. Loutfy, "The Electrolytic Production of Ti from a TiO2 Feed (The DARPA Sponsored Program)," in *Cost-Affordable Titanium Iii*, vol. 436, M. A. Imam, F. H. Froes, and K. F. Dring, Eds. Stafa-Zurich: Trans Tech Publications Ltd, 2010, pp. 61–74.

[5] Z. A. Munir, U. Anselmi-Tamburini, and M. Ohyanagi, "The effect of electric field and pressure on the synthesis and consolidation of materials: A review of the spark plasma sintering method," *J. Mater. Sci.*, vol. 41, no. 3, pp. 763–777, Feb. 2006.

[6] Y. Sun, K. Kulkarni, A. K. Sachdev, and E. J. Lavernia, "Synthesis of γ-TiAl by Reactive Spark Plasma Sintering of Cryomilled Ti and Al Powder Blend: Part II: Effects of Electric Field and Microstructure on Sintering Kinetics," *Metall. Mater. Trans. A*, vol. 45, no. 6, pp. 2759–2767, 2014.

[7] K. Kulkarni and A. Sachdev, "Multicomponent Titanium Aluminde Article and Method of Making," US 9061351 B2.

[8] Z. A. Munir, D. V. Quach, and M. Ohyanagi, "Electric Current Activation of Sintering: A Review of the Pulsed Electric Current Sintering Process," *J. Am. Ceram. Soc.*, vol. 94, no. 1, pp. 1–19, Jan. 2011.

[9] O. Guillon, J. Gonzalez-Julian, B. Dargatz, T. Kessel, G. Schierning, J. Räthel, and M. Herrmann, "Field-Assisted Sintering Technology/Spark Plasma Sintering: Mechanisms, Materials, and Technology Developments: FAST/SPS: Mechanisms, Materials, and Technology Developments," *Adv. Eng. Mater.*, vol. 16, no. 7, pp. 830–849, Jul. 2014.

[10] J. E. Garay, "Current-Activated, Pressure-Assisted Densification of Materials," in *Annual Review of Materials Research, Vol 40*, vol. 40, D. R. Clarke, M. Ruhle, and F. Zok, Eds. Palo Alto: Annual Reviews, 2010, pp. 445–468.

[11] Y. J. Liu, T. Y. Pan, L. J. Zhang, D. Yu, and Y. Ge, "Kinetic modeling of diffusion mobilities in bcc Ti-Nb alloys," *J. Alloys Compd.*, vol. 476, no. 1–2, pp. 429–435, May 2009.

[12] C. Leyens and M. Peters, *Titanium and titanium alloys*. Weinheim: Wiley-VCH, 2003.

[13] M. Donachie, *Titanium A Technical Guide*, Second Ed. Materials Park, OH: ASM International, 2000.

[14] A. E. Pontau and D. Lazarus, "Diffusion of titanium and niobium in bcc Ti-Nb alloys," p. 11.

[15] G. B. Gibbs, D. Graham, and D. H. Tomlin, "Diffusion in titanium and titanium—niobium alloys," *Philos. Mag.*, vol. 8, no. 92, pp. 1269–1282, Aug. 1963.

[16] V. Verma and K. Kulkarni, "Investigations of Interdiffusion in Titanium-Niobium Alloys," *Mater. Sci. Technol. MST*, p. 8, 2015.

[17] A. Paul, T. Laurila, V. Vuorinen, and S. V. Divinski, *Thermodynamics, Diffusion and the Kirkendall Effect in Solids*. Cham: Springer International Publishing, 2014.
[18] J. Crank, *The mathematics of diffusion*, 2d ed. Oxford, [Eng]: Clarendon Press, 1975.
[19] H. Conrad, "Effects of electric current on solid state phase transformations in metals," *Mater. Sci. Eng. -Struct. Mater. Prop. Microstruct. Process.*, vol. 287, no. 2, pp. 227–237, Aug. 2000.
[20] R. E. Hummel, "Electromigration in integrated circuit components," *Int. Mater. Rev.*, vol. 39, no. 9, pp. 97–111, 1994.
[21] S. W. Chen, C. M. Chen, and W. C. Liu, "Electric current effects upon the Sn/Cu and Sn/Ni interfacial reactions," *J. Electron. Mater.*, vol. 27, no. 11, pp. 1193–1198, Nov. 1998.
[22] J. E. Garay, S. C. Glade, U. Anselmi-Tamburini, P. Asoka-Kumar, and Z. A. Munir, "Electric current enhanced defect mobility in Ni3Ti intermetallics," *Appl. Phys. Lett.*, vol. 85, no. 4, pp. 573–575, Jul. 2004.
[23] C. Yang, J. A. Lin, Y. F. Ding, W. W. Zhang, Y. Y. Li, Z. Q. Fu, F. Chen, and E. J. Lavernia, "Texture evolution and mechanical behavior of commercially pure Ti processed via pulsed electric current treatment," *J. Mater. Sci.*, vol. 51, no. 23, pp. 10608–10619, Dec. 2016.
[24] Y. Sun, J. Haley, K. Kulkarni, M. Aindow, and E. J. Lavernia, "Influence of electric current on microstructure evolution in Ti/Al and Ti/TiAl3 during spark plasma sintering," *J. Alloys Compd.*, vol. 648, pp. 1097–1103, Nov. 2015.
[25] S. Paul, *Diffusion in Solids*, Second. Ohio State University: TMS, 1989.
[26] Y. Minamino, T. Yamane, Akio Shimomura, M. Shimada, M. Koizumi, N. Ogawa, J. Takahashi, and H. Kimura. "Effect of high pressure on interdiffusion in an Al-Mg alloy," *J. Mater. Sci.*, vol. 18, no. 9, pp. 2679–2687, Sep. 1983.
[27] R. N. Jeffery, "Effect of High Pressure on Self-Diffusion in Beta-Titanium," *Phys. Rev. B*, vol. 3, no. 12, pp. 4044–4055, Jun. 1971.
[28] U. Anselmi-Tamburini and J. R. Groza, "Critical assessment: electrical field/current application – a revolution in materials processing/sintering?," *Mater. Sci. Technol.*, vol. 33, no. 16, pp. 1855–1862, Nov. 2017.
[29] J. E. Alaniz, A. D. Dupuy, Y. Kodera, and J. E. Garay, "Effects of applied pressure on the densification rates in current-activated pressure-assisted densification (CAPAD) of nanocrystalline materials," *Scr. Mater.*, vol. 92, pp. 7–10, Dec. 2014.
[30] C. Yang, D.G. Mo, H.Z. Lu, X.Q. Li, W.W. Zhang, Z.Q. Fu, L.C. Zhang, and E.J. Lavernia, "Reaction diffusion rate coefficient derivation by isothermal heat treatment in spark plasma sintering system," *Scr. Mater.*, vol. 134, pp. 91–94, Jun. 2017.
[31] J. Zhao, J. E. Garay, U. Anselmi-Tamburini, and Z. A. Munir, "Directional electromigration-enhanced interdiffususion in the Cu–Ni system," *J. Appl. Phys.*, vol. 102, no. 11, p. 114902, 2007.
[32] C. Wang, L. F. Cheng, and Z. Zhao, "FEM analysis of the temperature and stress distribution in spark plasma sintering: Modelling and experimental validation," *Comput. Mater. Sci.*, vol. 49, no. 2, pp. 351–362, Aug. 2010.
[33] Wesley A. Salandro, Joshua J. Jones, Cristina Bunget, Laine Mears, and John T. Roth, *Electrically Assisted Forming Modeling and Control*. Springer International Publishing, 2015.

[34] M. A. Dayananda, “Analysis of multicomponent diffusion couples for interdiffusion fluxes and interdiffusion coefficients,” *J. Phase Equilibria Diffus.*, vol. 26, no. 5, pp. 441–446, Oct. 2005.
[35] S. Prasad and A. Paul, “Interdiffusion in Nb-Mo, Nb-Ti and Nb-Zr Systems,” *Defect Diffus. Forum*, vol. 323–325, pp. 491–496, Apr. 2012.
[36] P. Asoka-kumar, K. Obrien, K. G. Lynn, P. J. Simpson, and K. P. Rodbell, “Detection of current-induced vacancies in thin aluminum-copper lines using positrons,” *Appl. Phys. Lett.*, vol. 68, no. 3, pp. 406–408, Jan. 1996.
[37] X. Gao, S. Chen, F. Dong, L. Hu, R. Yang, W. Wang, and Z. A. Munir “Diffusion bonding of Ti/Ni under the influence of an electric current: mechanism and bond structure,” *J. Mater. Sci.*, vol. 52, no. 6, pp. 3535–3544, Mar. 2017.